Efficient Computation of the Near-Field Mutual Coupling Between Antennas on Vehicles

HENRIK FRID

KTH Electrical Engineering

Master's Degree Project
Stockholm, Sweden June 2014

XR-EE-EE 2014:002

This thesis work was carried out at Saab Electronic Defense Systems in Stockholm during the spring of 2014. The project was supervised by Henrik Holter at Saab and Lars Jonsson at KTH.

Contact:
Henrik Frid
hfrid@kth.se

KTH Electrical Engineering

Efficient Computation of the Near-Field Mutual Coupling Between Antennas on Vehicles

HENRIK FRID

Stockholm 2014

Electromagnetic Engineering
School of Electrical Engineering
Kungliga Tekniska Högskolan

XR-EE-EE 2014:002

Sammanfattning

En närfältsgeneralisering av Friis transmissionsekvation har tidigare föreslagits i litteraturen. Med denna generalisering kan den ömsesidiga kopplingen mellan två antenner beräknas som en viktad integral över antennernas fjärrfältsamplituder. I denna rapport används ett variabelbyte för att ta bort singulariteten i integranden och en normering av fjärrfältsamplituden föreslås för att ta hänsyn till antennernas förluster. Den resulterande icke-singulära integralen har implementerats i ett datorprogram som kan användas för att beräkna kopplingen mellan två godtyckligt polariserade antenner givet antennernas fjärrfältsamplituder och geometriska separation. Programmet har flera fördelar jämfört med tidigare program som baserats på närfältsgeneraliseringen av Friis transmissionsekvation. För det första kan detta program användas för att beräkna kopplingen mellan två godtyckligt polariserade och orienterade antenner då tidigare program har varit skrivna för linjärpolariserade och polarisationsmatchade antenner. Dessutom uppnås en högre numerisk stabilitet eftersom den icke-singulära formen av integralen används. Det demonstreras i flera exempel att kopplingen som beräknats med detta program för antenner som befinner sig i varandras närfält stämmer väl överens med resultat som beräknats med kommersiell mjukvara. Avslutningsvis undersöks om denna närfältsgeneralisering kan användas för att approximativt beräkna kopplingen mellan två antenner på en elektriskt stor farkost.

Nyckelord: Närfält, elektromagnetisk interferens, antenner

Abstract

A near-field generalization of Friis transmission equation has previously been proposed in the literature. Using this generalization, it is possible to calculate the mutual coupling between two antennas as a weighted integral over the antenna far-fields. In this thesis, a change of variables is used to remove the singularity in the integrand and a normalization of the antenna far-field is suggested to take mismatch and thermal losses into account. The resulting non-singular integral has been implemented in a computer program that can be used to calculate the mutual coupling between two arbitrarily polarized antennas given the antenna far-fields and the geometrical separation between the antennas. The program has several advantages compared to previous programs based on the near-field generalization of Friis transmission equation. Firstly, this program can calculate the mutual coupling between two arbitrarily polarized and oriented antennas whereas previous programs could only be used for linearly polarized and polarization-matched antennas. Secondly, the advantage of the non-singular form is the improved numerical stability. The mutual coupling calculated using this program is demonstrated to agree well with results from full three-dimensional simulations of antennas located in each others near-fields using commercial software. Finally, we investigate for the first time if this integral relation can be used to calculate approximate values of the mutual coupling between antennas on an electrically large vehicle.

Keywords: Near-field, electromagnetic interference, antennas

Acknowledgements

Firstly, I wish to thank Henrik Holter for giving me the opportunity to join Saab Electronic Defense Systems during this thesis work and for suggesting a project with a strong emphasis on theory. I would also like to thank Henrik Holter and Lars Jonsson for several interesting discussions during the project. Although it is not possible to mention them all, I would like to express my sincere gratitude to a large number of people from several departments of the Royal Institute of Technology, who have to various extent contributed to the success of my education and subsequent research. Finally, I wish to thank my friends and family who have supported me throughout my time at KTH.

Notation

The notation used in this thesis is consistent with the notation used in most textbooks on electromagnetic theory, e.g. [1–3]. Hence, scalars are denoted by italic letters (a, b, c, ...) and vectors are denoted by bold italic letters ($\boldsymbol{a}$, $\boldsymbol{b}$, $\boldsymbol{c}$, ...). The position vector is denoted by $\boldsymbol{r}$ and the wave vector is denoted by $\boldsymbol{k}$. Note also that $k \equiv |\boldsymbol{k}| = 2\pi/\lambda = \omega/c$ etc. Unit vectors are denoted by $\hat{\boldsymbol{a}} \equiv \boldsymbol{a}/a$. The azimuthal and polar angles in the spherical system of coordinates are denoted by ϕ and θ respectively. The imaginary unit is denoted by i when the time convention $e^{-i\omega t}$ and by j when the time convention $e^{j\omega t}$ is used.

Contents

Chapter 1

Introduction

In order to accurately measure antenna properties in the far-field, the measurement probe should be located at least a distance $2D^2/\lambda$ from the antenna under test (AUT) where D is the diameter of the smallest sphere enclosing the radiating parts of the AUT and λ is the wavelength [2,4]. This limitation can in many cases be impractical, particularly for electrically large antennas such as array or reflector antennas. A significant amount of research has therefore been aimed at investigating if antenna far-field properties can be estimated from measurements in the near-field. Kerns and Dayhoff [5] were the first researchers to do an efficient transformation from the near-field to the far-field when scanning the near-field in a planar geometry in front of the AUT [4]. The transformation from near-field to far-field can today be done efficiently only for three scanning area geometries: planar, cylindrical and spherical [4, 6].

The inverse problem of finding the antenna near-fields given their far-fields was given very little attention until Yaghjian [7] used the plane-wave scattering matrix description of antennas [8, 9] to show that it is possible to calculate the near-field mutual coupling between antennas given only the antenna far-fields and the geometrical separation between the antennas. This paper also demonstrated that the method can be used to calculate the electric field strength in the near-field region given only the antenna far-field. Further work showed excellent agreement between measured and calculated electric field magnitudes in the near-field region using this method [10]. Additional research has shown that it is possible to locate the position of radome defects by reconstructing equivalent currents from near-field measurements [11] and far-field measurements [12, 13].

Another problem which can potentially be solved using far-field data is to estimate the mutual coupling between antennas on electrically large vehicles. Calculating the mutual coupling between antennas is a practically important problem in the development of military aircrafts which typically have a large number of closely placed antennas used for communication, GPS, radar and electronic warfare. The number of antennas can reach up to 60 per aircraft [14]. There are several criteria for antennas installed on an aircraft. Firstly, their installed radiation patterns need to satisfy some criteria for beamwidth, sidelobe

level, polarization etc. Secondly, a good isolation, i.e. a small mutual coupling, is required between certain antennas. In particular, a good isolation is required between transmitting and receiving antennas in order to achieve a strong signal-to-noise ratio (SNR) for received signals. Aircrafts are however electrically large for frequencies around and above 2 GHz and vast computational resources would therefore be required for solving the full three-dimensional problem of calculating the mutual coupling between antennas on an aircraft at high frequencies. Many antennas, particularly for radar and electronic warfare applications, operate in the frequency band $2 - 18$ GHz and there is thus a demand for fast methods to calculate the mutual coupling between antennas at high frequencies. The aim of this thesis is therefore to develop an approximate method for calculating the mutual coupling between antennas on electrically large vehicles when the antenna far-fields are known.

Traditionally, the mutual coupling between two antennas in free space is calculated using Friis transmission equation if the antenna separation is sufficiently large for the antennas to be located in each others far-fields (see [15] or e.g. [2]). There are however two main issues with using Friis transmission equation to calculate the mutual coupling between antennas on a vehicle. Firstly, the antennas are often closely placed and near-field contributions to the mutual coupling can not be neglected. Attempts have been made to extend the validity of Friis transmission equation to the near-field by taking into account the gain reduction factor and an empirical coefficient [16]. Yaghjian proposed an integral relation between the near-field mutual coupling and the antenna far-fields [7]. This integral relation has been referred to as a near-field counterpart of Friis transmission equation [17]. Friis transmission equation takes into account the receiving and transmitting properties of the antennas in only one direction whereas the near-field generalization takes these properties into account for all directions. This near-field generalization is exact when neglecting multiple reflections and evanescent modes. Excellent agreement with measurements have been found for linearly polarized antennas [17–20].

The second issue with using Friis transmission equation for antennas on a large vehicle is that it does not take into account any surface currents induced in the surface between the antennas. These currents can be taken into account to some extent by using the installed far-fields when calculating the mutual coupling between the antennas. In this thesis we therefore investigate if it is possible to calculate approximate values of the mutual coupling between antennas on a vehicle by using the installed far-fields as input to the integral from [7]. This integral relation is exact in the near-field when neglecting multiple reflections and evanescent modes and the approximation therefore lies only in the fact that the antennas are not truly in free space. A major part of the work is focused on the correct implementation of the results from [7] in a computer program hereafter referred to as the *coupling program*. This approximate method is finally used for some example configurations and the results are discussed.

Two methods have been proposed for efficient computation of this integral. The first method is based on the Fast Fourier Transform (FFT) and the second method is based on a series expansion of the integral [7, 18, 19]. The resulting

computer programs have previously only been evaluated for linearly polarized antennas [17–20]. In this thesis we demonstrate that this integral relation is valid also for antennas with an arbitrary polarization, provided that the antenna far-fields are treated correctly. The integral relation in [7] is singular. This singularity can be removed by calculating the integral using the previously mentioned series expansion rather than by direct numerical integration [7, 17]. However, this series expansion does not converge for very small antenna separations [7]. We therefore propose a novel change of variables to remove this singularity and thus providing a greater numerical stability of the integral. This modified integral relation, referred to as the non-singular coupling integral, is demonstrated to have very good agreement with simulation results using the commercial software CST Microwave Stuido [21]. Finally, we investigate if this integral relation is useful for calculating the mutual coupling between antennas on a large conducting vehicle.

The thesis is outlined as follows: Chapter 2 presents the theoretical aspects of this work. The near-field generalization of Friis transmission equation from [7] is presented in Section 2.1. By analyzing the integral in the far-field limit, we arrive at an alternative derivation of Friis transmission equation in Section 2.2. In this section, we also derive a normalization of the far-fields in order to take thermal and reflection losses into account. The series expansion of this integral is derived in Section 2.3 and the change of variables to remove the singularity in the original integral is presented in Section 2.5. In Chapter 3, this integral is calculated for some antenna configurations using analytical far-fields. Chapter 4 treats the problems encountered when using measured or simulated far-fields rather than analytical far-fields. The mutual coupling between several antenna types is calculated in the near-field region and a good agreement is found with simulations using CST Microwave Studio. In Section 5.1 we demonstrate that this integral relation can be used to calculate the mutual coupling as function of frequency. Finally, the mutual coupling between two antennas on a large conducting object is calculated in Section 5.2.

Chapter 2

Near-field generalization of Friis transmission equation

2.1 The coupling integral

Consider a two-port network consisting of two antennas placed a distance P from each other in free space according to Fig. 2.1 and Fig. 2.2. A global system of coordinates is chosen such that the origin coincides with the position of one of the antennas. The variables corresponding to this antenna are denoted with index t (transmitter) whereas the variables of the other antenna are denoted with index r (receiver). The voltage (or waveguide mode coefficient) into the transmitting antenna is thus denoted by a_t and the voltage out of the port of the second antenna is denoted by b_t. If the system is isolated and the receiving antenna is terminated in a matched load, then $|b_\mathrm{r}|^2/|a_\mathrm{t}|^2$ is the ratio of received to transmitted power. This ratio is often referred to as the *coupling ratio* or the *mutual coupling* between the antennas. Using the conventional scattering matrix for a two-port network, this is equivalent to $|S_{21}|^2$ [3]. Due to the reciprocity theorem for two antennas [2] this is also equivalent to $|S_{12}|^2$. In order to reduce the interference between two closely placed antennas, this ratio should be as small as possible. In addition to the global system of coordinates introduced in Fig. 2.2 there is also a local coordinate system used for each antenna. These systems are referred to as $S_\mathrm{t} = \{x_\mathrm{t},\ y_\mathrm{t},\ z_\mathrm{t},\ O_\mathrm{t}\}$ and $S_\mathrm{r} = \{x_\mathrm{r},\ y_\mathrm{r},\ z_\mathrm{r},\ O_\mathrm{r}\}$ for the transmitting and receiving antennas respectively and are presented in Fig. 2.1.

Consider now one antenna in a local coordinate system such that the antenna is placed in $\boldsymbol{r} = 0$. In the antenna far-field region, which is defined by $kr \gg 1$, the electric field has the following general form:

$$\boldsymbol{E}(\boldsymbol{r}) \approx \frac{e^{\pm ikr}}{r} V_0 \boldsymbol{f}(\hat{\boldsymbol{r}}) \tag{2.1}$$

where the choice of sign in the exponential depends on the choice of harmonic

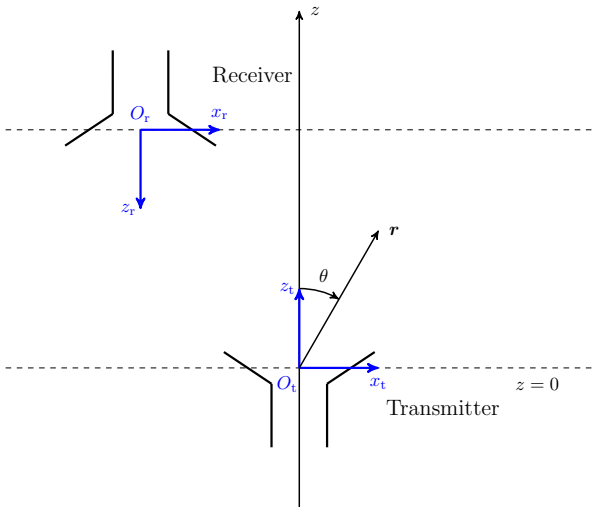

Figure 2.1: Illustration of the local systems of coordinates $S_t = \{x_t,\ y_t,\ z_t,\ O_t\}$ and $S_r = \{x_r,\ y_r,\ z_r,\ O_r\}$ (blue) for two arbiratily positioned antennas.

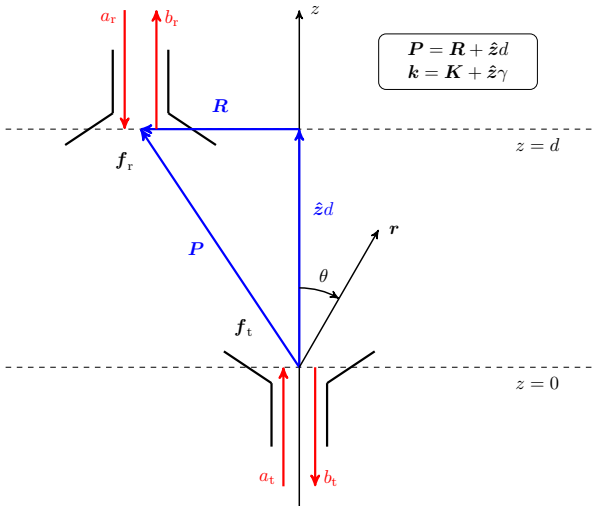

Figure 2.2: Illustration of two antennas separated by a vector $\boldsymbol{P}$ (blue) with complex voltage amplitudes (red) and system of coordinates (black). The antennas may have arbitrary orientation depending on the choice of normalized far-fields ($\boldsymbol{f}_t$ and $\boldsymbol{f}_r$ respectively).

time-dependence ($e^{-i\omega t}$ or $e^{+j\omega t}$ for + and − respectively) [1, 4]. This relation is proven in Appendix B. Using (2.1), it is possible to uniquely describe the electric far-field using the normalized vector far-field function:

$$\boldsymbol{f}(\theta,\phi) \equiv \frac{1}{V_0} \lim_{r\to\infty} re^{\mp ikr}\boldsymbol{E}(\boldsymbol{r}) \tag{2.2}$$

where V_0 is a constant of the dimension voltage. This function is commonly denoted by both $\boldsymbol{f}(\hat{\boldsymbol{r}})$ and $\boldsymbol{f}(\boldsymbol{k})$ in the literature depending on the context. In order to avoid confusion over this notation, it is important to note that by $\boldsymbol{f}(\theta,\phi), \boldsymbol{f}(\hat{\boldsymbol{r}})$ and $\boldsymbol{f}(\boldsymbol{k})$ all refer to the normalized far-field as function of the spherical angles for one choice of angular frequency, i.e. $\boldsymbol{f}(\theta,\phi;\ \omega)$. This frequency dependence is often omitted in order to use a short notation. The normalized far-field $\boldsymbol{f}(\theta,\phi)$ describes the transmitting and receiving characteristics of the antenna. In particular, if V_0 is chosen equal to

$$V_D = \sqrt{\frac{1}{4\pi}\int_\Omega \lim_{r'\to\infty} |r'\boldsymbol{E}(\boldsymbol{r}')|^2 \sin\theta' d\theta' d\phi'} \tag{2.3}$$

where $\Omega = \{(\theta,\ \phi) \in \mathbb{R}^2;\ 0 < \theta < \pi,\ 0 < \phi < 2\pi\}$ is the unit sphere, then $|\boldsymbol{f}(\theta,\phi)|^2$ equals the antenna directivity $D(\theta,\phi)$ [2].

If the antennas in Fig. 2.2 are located in each others far-fields, the ratio of received to transmitted power can be estimated using Friis transmission equation (see [15] or e.g. [2]):

$$\left|\frac{b_\mathrm{r}}{a_\mathrm{t}}\right|^2 = e_\mathrm{t}e_\mathrm{r}(1-|\Gamma_\mathrm{t}|^2)(1-|\Gamma_\mathrm{r}|^2)D_\mathrm{t}(\theta_\mathrm{t},\phi_\mathrm{t})D_\mathrm{r}(\theta_\mathrm{r},\phi_\mathrm{r})\left(\frac{\lambda}{4\pi P}\right)^2 |\hat{\boldsymbol{n}}_\mathrm{t}\cdot\hat{\boldsymbol{n}}_\mathrm{r}^*|^2 \tag{2.4}$$

where

e_t	=	Loss factor for transmitting antenna
e_r	=	Loss factor for receiving antenna
Γ_t	=	Reflection factor (S_{11}) for the transmitting antenna
Γ_r	=	Reflection factor (S_{11}) for the receiving antenna
$\hat{\boldsymbol{n}}_\mathrm{t}$	=	Unit polarization vector for the transmitting antenna
$\hat{\boldsymbol{n}}_\mathrm{r}$	=	Unit polarization vector for the receiving antenna
D_t	=	Directivity of transmitting antenna
D_r	=	Directivity of receiving antenna

This relation can be understood intuitively. In particular, the factor $(1/P)^2$ is a result of the power transmitted by the transmitting antenna spreading out over a spherical surface. Some of the transmitted power is collected by the effective area of the receiving antenna. This relation can be recognized as the "inverse square law" that occurs in a large number of fields in physics. The distance r_f which is found from

$$r_f = 2\frac{(D')^2}{\lambda} \tag{2.5}$$

where D' is the diameter of the smallest sphere enclosing the radiating parts of the antenna is often used as a "starting point" of the far-field [2, 4]. When

calculating the mutual coupling between two antennas, the size of both the receiver and the transmitter need to be taken into account and the following condition is then sometimes used:

$$P > P_f = \frac{(D'_{\mathrm{t}} + D'_{\mathrm{r}})^2}{\lambda} \tag{2.6}$$

where D'_{t} and D'_{r} are the greatest dimensions of the transmitting and receiving antenna respectively [7].

The conjugate in the polarization mismatch factor $|\hat{\boldsymbol{n}}_{\mathrm{t}} \cdot \hat{\boldsymbol{n}}^*_{\mathrm{r}}|^2$ in (2.4) is crucial when defining right-hand circular polarization (RHCP) with the polarization unit vector $\hat{\boldsymbol{n}}_{\mathrm{RHCP}} = (\hat{\boldsymbol{\theta}} + i\hat{\boldsymbol{\phi}})/\sqrt{2}$ and left-hand circular polarization (LHCP) with $\hat{\boldsymbol{n}}_{\mathrm{LHCP}} = (\hat{\boldsymbol{\theta}} - i\hat{\boldsymbol{\phi}})/\sqrt{2}$ for the time dependence $e^{-i\omega t}$ and an outwards propagating spherical wave. If the receiving antenna has RHCP and the transmitting antenna has LHCP, the mutual coupling between them should be zero when neglecting any unwanted cross polarization. This is only satisfied if the conjugate in the polarization mismatch factor is present. Furthermore, note that $\hat{\boldsymbol{n}}_{\mathrm{RHCP}} = \hat{\boldsymbol{n}}^*_{\mathrm{LHCP}}$.

By introducing the realized gain G, (2.4) may be written in the following simple form [2]:

$$\left|\frac{b_{\mathrm{r}}}{a_{\mathrm{t}}}\right|^2 = G_{\mathrm{t}}(\theta_t, \phi_t) G_{\mathrm{r}}(\theta_r, \phi_r) \left(\frac{\lambda}{4\pi P}\right)^2 |\hat{\boldsymbol{n}}_{\mathrm{t}} \cdot \hat{\boldsymbol{n}}^*_{\mathrm{r}}|^2 \tag{2.7}$$

If the antennas are lossless and perfectly matched, then the directivity and the realized gain of the antennas are equivalent and either could therefore be used in (2.7).

A generalization of Friis transmission equation which is also valid in the near-field (where the antenna separation is smaller than r_f) was proposed by Yaghjian in [7], based on the Plane-Wave Scattering Matrix Theory by Kerns [8]. This generalization will be introduced in this chapter and it will be evaluated throughout this thesis. The harmonic time-dependence $e^{-i\omega t}$ was used in the original literature and will therefore be used also in this section. The case where the time-dependence is $e^{+j\omega t}$ is discussed in Section 2.4.

According to Fig. 2.2, the antenna separation $\boldsymbol{P}$ is now divided into two perpendicular components:

$$\boldsymbol{P} = \boldsymbol{R} + \hat{\boldsymbol{z}} d \tag{2.8}$$

where $\boldsymbol{R} \cdot \hat{\boldsymbol{z}} = 0$. Similarly, the wave vector is given by $\boldsymbol{k} = \boldsymbol{K} + \gamma \hat{\boldsymbol{z}}$ where $\boldsymbol{K} = k_x \hat{\boldsymbol{x}} + k_y \hat{\boldsymbol{y}}$. From $k^2 = K^2 + \gamma^2$ it follows that $\gamma = \sqrt{k^2 - K^2}$ where $k = 2\pi/\lambda = \omega/c$. γ is chosen real and positive for $K < k$. The integral relation between the antenna far-fields and the mutual coupling from [7] is given by:

$$\boxed{\frac{b_{\mathrm{r}}}{a_{\mathrm{t}}} = -\frac{C'}{k} \int_{K<k} \frac{\boldsymbol{f}_{\mathrm{r}}(-\boldsymbol{k}) \cdot \boldsymbol{f}_{\mathrm{t}}(\boldsymbol{k})}{\gamma} e^{i\gamma d} e^{i\boldsymbol{K}\cdot\boldsymbol{R}} d^2K} \tag{2.9}$$

This integral relation will hereafter be referred to as the *coupling integral*. It has been framed in a rectangular box in order to emphasize its importance in this

thesis. The integral relation (2.9) is derived by neglecting multiple reflections. Furthermore, it is valid for separation distances beyond "encroachment" i.e. for separation distances sufficiently large to ensure that a plane perpendicular to the z-axis may be placed between the two antennas in free space without intersecting either antenna [7].

The coefficient $-C'$ in (2.9) takes reflection losses into account. The normalization of $\boldsymbol{f}_{\mathrm{r}}$ and $\boldsymbol{f}_{\mathrm{t}}$ has not yet been specified and the coefficient $-C'$ can therefore be embedded in the dot product by choice of V_0. The resulting value of V_0 is derived in Section 2.2.

There are several strategies to evaluate the coupling integral (2.9) for sampled (measured of simulated) far-fields. Firstly, note that this integral is in fact a two-dimensional Fourier transform from the $\boldsymbol{K}$-space to the $\boldsymbol{R}$-space [7,22,23]. Hence, it is possible to rapidly calculate this integral for a set of values of $\boldsymbol{R}$ using the Fast Fourier Transform (FFT) [24, 25]. Another method is to express the coupling integral as a series in spherical Hankel functions and spherical harmonics [7, 17]. Finally, it should be noted that the integral is only taken over the visible part of the $\boldsymbol{K}$-space, thus neglecting evanescent modes [2, 7].

2.2 Asymptotic behavior of the coupling integral

In order for the coupling integral (2.9) to be a valid generalization of Friis transmission equation, it needs to have the asymptotic behavior (2.4) in the far-field limit $kP \gg 1$. The asymptotic behavior of this type of integrals may be analyzed using the method of stationary phase [2, 20]. By analyzing the coupling integral in the asymptotic limit $kP \gg 1$ similarly to [20], we arrive at an alternative derivation of Friis transmission equation in this section.

According to the method of stationary phase (see particularly Section 12.9.3 and Appendix VIII in [2]), integrals of the type

$$\xi(\boldsymbol{P}) = \frac{1}{4\pi^2} \int_{-\infty}^{\infty} \int_{-\infty}^{\infty} \chi(k_x, k_y) e^{i\boldsymbol{k}\cdot\boldsymbol{P}} dk_x dk_y \tag{2.10}$$

have the following asymptotic behavior in the the limit $kP \gg 1$:

$$\xi(\boldsymbol{P}) \approx (-i) \frac{k e^{ikP}}{2\pi P} \cos\theta_P \ \chi(k \sin\theta_P \cos\phi_P, k \sin\theta_P \sin\phi_P) \tag{2.11}$$

In this asymptotic approximation we use $\boldsymbol{k} = k\hat{\boldsymbol{P}}$, i.e.

$$\begin{aligned} k_x &= k \sin\theta_P \cos\phi_P \\ k_y &= k \sin\theta_P \sin\phi_P \\ k_z &\equiv \gamma = k \cos\theta_P \end{aligned} \tag{2.12}$$

where θ_P and ϕ_P are the polar and azimuthal angles describing $\boldsymbol{P}$ in the system of coordinates from Fig. 2.2.

By including the invisible region of the integration domain in (2.9), we can use (2.11) to analyze this integral in the asymptotic limit $kP \gg 1$:

$$\begin{aligned}\frac{b_\mathrm{r}}{a_\mathrm{t}} &= \frac{1}{k}\int_{\boldsymbol{K}\in\mathbb{R}^2} \frac{\boldsymbol{f}_\mathrm{r}(-\boldsymbol{k})\cdot\boldsymbol{f}_\mathrm{t}(\boldsymbol{k})}{\gamma} e^{i\gamma d} e^{i\boldsymbol{K}\cdot\boldsymbol{R}} d^2K \\ &\approx 2\pi(-i)\frac{ke^{ikP}}{P}\cos\theta_P \frac{\boldsymbol{f}_\mathrm{r}(-\hat{\boldsymbol{P}})\cdot\boldsymbol{f}_\mathrm{t}(\hat{\boldsymbol{P}})}{k\gamma} \\ &= -2\pi i \boldsymbol{f}_\mathrm{r}(-\hat{\boldsymbol{P}})\cdot\boldsymbol{f}_\mathrm{t}(\hat{\boldsymbol{P}})\frac{e^{ikP}}{kP}\end{aligned} \tag{2.13}$$

Taking the square magnitude of this equation:

$$\left|\frac{b_\mathrm{r}}{a_\mathrm{t}}\right|^2 = \left(\frac{\lambda}{P}\right)^2 |\boldsymbol{f}_\mathrm{r}(-\hat{\boldsymbol{P}})|^2 |\boldsymbol{f}_\mathrm{t}(\hat{\boldsymbol{P}})|^2 |\hat{\boldsymbol{n}}_\mathrm{t}\cdot\hat{\boldsymbol{n}}_\mathrm{r}^*|^2 \tag{2.14}$$

By comparing with (2.7) we find:

$$\left(\frac{\lambda}{4\pi P}\right)^2 (4\pi)^2 |\boldsymbol{f}_\mathrm{r}(-\hat{\boldsymbol{P}})|^2 |\boldsymbol{f}_\mathrm{t}(\hat{\boldsymbol{P}})|^2 = \left(\frac{\lambda}{4\pi P}\right)^2 G_\mathrm{t}(-\hat{\boldsymbol{P}}) G_\mathrm{r}(\hat{\boldsymbol{P}}) \tag{2.15}$$

i.e.

$$|\boldsymbol{f}(\theta,\phi)|^2 = \frac{1}{4\pi} G(\theta,\phi) \tag{2.16}$$

The normalization (2.16) will be used through this thesis. Finally, comparing with (2.3) it is clear that the following normalization should be used for lossless and perfectly matched antennas:

$$|V_0|^2 = \int_\Omega \lim_{r'\to\infty} |r'\boldsymbol{E}(\boldsymbol{r}')|^2 \sin\theta' d\theta' d\phi'. \tag{2.17}$$

2.3 Expansion of the coupling integral in spherical harmonics and spherical Hankel functions

An interesting property of the coupling integral (2.9) is that it satisfies the Helmholtz equation (2.21) [7, 17]. This will now be proven. The results and derivations in this section follow from and expand upon [7, 17]. The Laplacian operator is defined as

$$\nabla_P^2 \equiv \frac{\partial}{\partial P_i}\frac{\partial}{\partial P_i} \tag{2.18}$$

using Einstein's summation convention [26]. Operating on (2.9) with the Laplacian operator yields:

$$\nabla_P^2 \frac{b_\mathrm{r}}{a_\mathrm{t}} = \frac{1}{k}\int_{K<k} \frac{\boldsymbol{f}_\mathrm{r}(-\boldsymbol{k})\cdot\boldsymbol{f}_\mathrm{t}(\boldsymbol{k})}{\gamma} \nabla_P^2 e^{i\boldsymbol{k}\cdot\boldsymbol{P}} d^2K \tag{2.19}$$

where

$$\nabla_P^2 e^{i\boldsymbol{k}\cdot\boldsymbol{P}} = \frac{\partial}{\partial P_i}\frac{\partial}{\partial P_i} e^{ik_j P_j} = (ik_i)(ik_i)e^{i\boldsymbol{k}\cdot\boldsymbol{P}} = -k^2 e^{i\boldsymbol{k}\cdot\boldsymbol{P}} \tag{2.20}$$

By substituting (2.20) and (2.9) into equation (2.19), we find

$$(\nabla_P^2 + k^2)\frac{b_{\mathrm{r}}}{a_{\mathrm{t}}} = 0 \tag{2.21}$$

and the proof is thus complete.

Let a function $T(k\boldsymbol{P})$ satisfy the Helmholtz equation (2.21). Then $T(k\boldsymbol{P})$ may be expanded according to [1, 27, 28]:

$$T(k\boldsymbol{P}) = \sum_{l=0}^{\infty}\sum_{m=-l}^{l} a_{lm} F_l(kP) Y_{lm}(\theta_P, \phi_P) \tag{2.22}$$

where

$$\mathrm{Y}_{lm}(\theta,\phi) = \sqrt{\frac{2l+1}{4\pi}\frac{(l-m)!}{(l+m)!}}\mathrm{P}_l^m(\cos\theta)e^{im\phi} \tag{2.23}$$

are spherical harmonic functions and F_l is an arbitrary linear combination of spherical Bessel functions j_l and spherical Neumann functions n_l of order l. In many applications, it is useful to introduce the spherical Hankel functions of the first and second kind respectively:

$$\begin{aligned} \mathrm{h}_l^{(1)}(kP) &= \mathrm{j}_l(kP) + i\mathrm{n}_l(kP) \\ \mathrm{h}_l^{(2)}(kP) &= \mathrm{j}_l(kP) - i\mathrm{n}_l(kP) \end{aligned} \tag{2.24}$$

The usefulness of these functions lies in their asymptotic behavior in the limit $kP \gg l$:

$$\begin{aligned} \mathrm{h}_l^{(1)}(kP) &\approx (-i)^{l+1}e^{ikP}/kP \\ \mathrm{h}_l^{(2)}(kP) &\approx i^{l+1}e^{-ikP}/kP \end{aligned} \tag{2.25}$$

We now return to the asymptotic expression for the coupling integral (2.13):

$$\frac{b_{\mathrm{r}}}{a_{\mathrm{t}}} \approx -2\pi i \boldsymbol{f}_{\mathrm{r}}(-\hat{\boldsymbol{P}})\cdot\boldsymbol{f}_{\mathrm{t}}(\hat{\boldsymbol{P}})\frac{e^{ikP}}{kP}.$$

From (2.21) and (2.22) we have

$$\frac{b_{\mathrm{r}}}{a_{\mathrm{t}}} = \sum_{l=0}^{\infty}\sum_{m=-l}^{l} B_{lm} F_l(kP)\mathrm{P}_l^m(\cos\theta_P)e^{im\phi_P} \tag{2.26}$$

It is clear that $F_l(kP) = \mathrm{h}_l^{(1)}(kP)$ is required in order for (2.26) to have the correct asymptotic behavior in the limit $kP \gg l$, i.e.

$$\frac{b_{\mathrm{r}}}{a_{\mathrm{t}}} \approx \sum_{l=0}^{\infty}\sum_{m=-l}^{l} B_{lm}\frac{(-i)^{l+1}e^{ikP}}{kP}P_l^m(\cos\theta_P)e^{im\phi_P} \tag{2.27}$$

By equating (2.27) and (2.13) in the asymptotic limit we find:

$$\sum_{l=0}^{\infty}\sum_{m=-l}^{l} B_{lm}\frac{(-i)^{l+1}e^{ikP}}{kP}P_l^m(\cos\theta)e^{im\phi} = -2\pi i\boldsymbol{f}_{\mathrm{r}}(-\hat{\boldsymbol{P}})\cdot\boldsymbol{f}_{\mathrm{t}}(\hat{\boldsymbol{P}})\frac{e^{ikP}}{kP} \quad (2.28)$$

By multiplying this equation by $\mathrm{P}_n^{m'}(\cos\theta_P)e^{-im'\phi_P}$ and integrating over the unit sphere, we can use the orthogonality of the associated Legendre functions [1, 28, 29]

$$\int_0^{\pi} P_n^m(\cos\theta)P_l^m(\cos\theta)\sin\theta d\theta = \int_{-1}^{1} P_n^m(x)P_l^m(x)dx = \frac{(n+m)!}{(n-m)!}\frac{2}{2n+1}\delta_{nl} \quad (2.29)$$

and

$$\int_0^{2\pi} e^{i(m-m')\phi}d\phi = 2\pi\delta_{mm'} \quad (2.30)$$

to find

$$B_{nm} = \frac{1}{(-i)^n}\frac{2n+1}{2}\frac{(n-m)!}{(n+m)!}\int_0^{2\pi}d\phi_P\int_0^{\pi}d\theta_P\sin\theta_P P_n^m(\cos\theta_P)e^{-im\phi_P} \boldsymbol{f}_{\mathrm{r}}(-\hat{\boldsymbol{P}})\cdot\boldsymbol{f}_{\mathrm{t}}(\hat{\boldsymbol{P}}). \quad (2.31)$$

We can choose a system of coordinates such that the antennas are oriented along the z-axis (Fig. 2.3) and we are therefore only interested in evaluating this series expansion on the z-axis where $\boldsymbol{R} = 0$. Using the identity

$$\mathrm{P}_l^m(\cos(0)) = \delta_{m0} \quad (2.32)$$

we find

$$\left.\frac{b_{\mathrm{r}}}{a_{\mathrm{t}}}\right|_{\boldsymbol{R}=0} = \lim_{L\to\infty}\sum_{n=0}^{L} B_n \mathrm{h}_n^{(1)}(kd) \quad (2.33)$$

where $B_n \equiv B_{n0}$:

$$B_n = i^n\frac{2n+1}{2}\int_0^{\pi}d\theta_P\int_0^{2\pi}d\phi_P\ \boldsymbol{f}_{\mathrm{r}}(-\hat{\boldsymbol{P}})\cdot\boldsymbol{f}_{\mathrm{t}}(\hat{\boldsymbol{P}})\mathrm{P}_n(\cos\theta_P)\sin\theta_P \quad (2.34)$$

The expansion (2.33) with coefficients (2.34) derived in this section is also found in [7]. In order to implement this series expansion in a computer program it is important to note that the normalization of the Legendre polynomials P_n is the same as (2.29) with $m = 0$.

There are some advantages to calculating the coupling integral (2.9) using the expansion derived in this section. In particular, the integrand in the coupling integral as given in the original literature is singular at $\gamma = 0$, but the integrand in (2.34) has no singular point. This method can therefore provide greater numerical stability than straightforward integration of (2.9) as it is given in

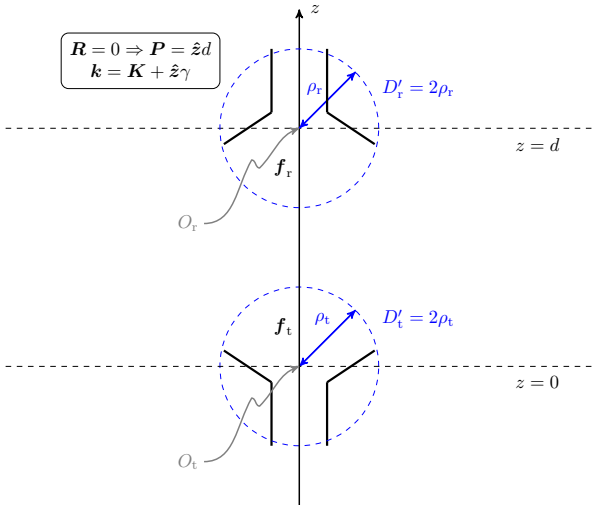

Figure 2.3: Illustration of two antennas in the configuration from Fig. 2.2. The system of coordinates is chosen such that $R = 0$. The antennas are bounded by hypothetical spheres with radii ρ_r and ρ_t respectively and may have arbitrary orientation depending on the choice of normalized far-fields ($\boldsymbol{f}_\mathrm{t}$ and $\boldsymbol{f}_\mathrm{r}$ respectively). O_t and O_r are the origins of the local system of coordinates S_t and S_r.

the literature. A novel method to remove the singularity in (2.9) is derived in Section 2.5.

The expansion derived in this section is valid for separation distances greater than [7]:

$$r_0 = \rho_\mathrm{r} + \rho_\mathrm{t} \tag{2.35}$$

where ρ_r and ρ_t are the radii of a sphere enclosing the sources in each antenna according to Fig. 2.3. Together with the rule of thumb (2.5), it is clear that the result from this series expansion is mainly interesting throughout the Fresnel region (the radiating near-field):

$$\frac{\rho_\mathrm{r} + \rho_\mathrm{t}}{\lambda} < \frac{d}{\lambda} < \left(\frac{D'_\mathrm{t} + D'_\mathrm{r}}{\lambda} \right)^2 \tag{2.36}$$

For numerical treatment of (2.33), it is necessary to truncate the series to a sum with a finite number of terms ($L < \infty$). The number of terms (modes) required in the expansion is according to [7]:

$$L \geq k(\rho_\mathrm{r} + \rho_\mathrm{t} + \lambda) \tag{2.37}$$

2.4 Changing the time dependence

The harmonic time-dependence $e^{-i\omega t}$ is assumed in (2.9). If the harmonic time-dependence $e^{+j\omega t}$ is used instead, the corresponding integral relation is found by changing the sign in the complex exponential according to:

$$\left(\frac{b_{\mathrm{r}}}{a_{\mathrm{t}}}\right)_{+} = \int_{K<k} \frac{1}{k\gamma} \boldsymbol{f}_{\mathrm{r}}(-\boldsymbol{k}) \cdot \boldsymbol{f}_{\mathrm{t}}(\boldsymbol{k}) e^{-j\boldsymbol{k}\cdot\boldsymbol{P}} d^2K \tag{2.38}$$

where the + is used to emphasize that the time convention $e^{+j\omega t}$ is used. By repeating the derivation from the previous section, the corresponding expansion is found:

$$\left(\frac{b_{\mathrm{r}}}{a_{\mathrm{t}}}\right)_{+,\boldsymbol{R}=0} = \lim_{L\to\infty} \sum_{n=0}^{L} (B_n)_{+} \, \mathrm{h}_n^{(2)}(kd) \tag{2.39}$$

where

$$(B_n)_{+} = (-j)^n \frac{2n+1}{2} \int_0^{\pi} d\theta_P \int_0^{2\pi} d\phi_P \;\; \boldsymbol{f}_{\mathrm{r}}(-\hat{\boldsymbol{P}}) \cdot \boldsymbol{f}_{\mathrm{t}}(\hat{\boldsymbol{P}}) \mathrm{P}_n(\cos\theta_P) \sin\theta_P \tag{2.40}$$

2.5 Non-singular coupling integral

In order to integrate (2.38) using numerical methods, it is advantageous to make a change of variables in order to remove the singularity in $\gamma = 0$. Using $K^2+\gamma^2 = k^2$ and $\gamma = k\cos\theta$ we make the change of variables $d^2K = KdKd\phi = -\gamma d\gamma d\phi = \gamma k \sin\theta d\theta d\phi$ and arrive at the following expression

$$\boxed{\left(\frac{b_{\mathrm{r}}}{a_{\mathrm{t}}}\right)_{+} = \int_0^{\pi/2} d\theta \int_0^{2\pi} d\phi \;\; \boldsymbol{f}_{\mathrm{r}}(-\boldsymbol{k}) \cdot \boldsymbol{f}_{\mathrm{t}}(\boldsymbol{k}) e^{-j\boldsymbol{K}\cdot\boldsymbol{R}} e^{-jkd\cos\theta} \sin\theta} \tag{2.41}$$

where $\boldsymbol{K}\cdot\boldsymbol{R} = (kR_x\cos\phi + kR_y\sin\phi)\sin\theta$. The singularity in the coupling integral has thus been removed. This is, to the author's best knowledge, a novel result. This integral will hereafter be referred to as the *non-singular coupling integral* (NSCI) and it will be evaluated for several antenna configurations in the following chapters. It should be noted that the limits of integration differ between the NSCI (2.41) and the coefficients in the corresponding series expansion (2.40).

2.6 Some practical aspects of the coupling integral

The first step when calculating the integrals in this chapter is to calculate the dot product $\boldsymbol{f}_{\mathrm{t}}(\boldsymbol{k})\cdot\boldsymbol{f}_{\mathrm{r}}(-\boldsymbol{k})$. It is however not always straightforward to calculate

$\boldsymbol{f}_{\mathrm{r}}(-\boldsymbol{k})$ due to the negative sign in the argument of $\boldsymbol{f}_{\mathrm{r}}$. For analytical far-fields, we can simply use the following mapping

$$\begin{aligned} \theta &\to \pi - \theta \\ \phi &\to \pi + \phi \end{aligned} \tag{2.42}$$

i.e. $\boldsymbol{f}_{\mathrm{r}}(-\boldsymbol{k}) \equiv \boldsymbol{f}_{\mathrm{r}}(\pi-\theta, \pi+\phi;\, \omega)$. In order to correctly evaluate the dot product for sampled far-fields, we must first note that the receiving factor $\boldsymbol{f}_{\mathrm{r}}(-\boldsymbol{k})$ may be written as $\boldsymbol{f}_{\mathrm{r}}(BA\boldsymbol{k})$ where $BA = -\mathrm{I}$ and I is the identity operator. In the Cartesian system of coordinates, these operators may be expressed as

$$A = \begin{pmatrix} 1 & 0 & 0 \\ 0 & -1 & 0 \\ 0 & 0 & -1 \end{pmatrix}, \quad B = \begin{pmatrix} -1 & 0 & 0 \\ 0 & 1 & 0 \\ 0 & 0 & 1 \end{pmatrix}. \tag{2.43}$$

The first operator (A) corresponds to a rotation 180° around the x-axis whereas the second operator (B) mirrors the vector $A\boldsymbol{k}$ in the yz-plane. Hence, we have decomposed the operator $-\mathrm{I}$ with respect to the unit vector $\hat{\boldsymbol{x}}$. We could choose any unit vector instead of $\hat{\boldsymbol{x}}$ and this decomposition is therefore not unique. This decomposition will be discussed further in Section 4.4.

When a conducting object is placed a distance P from a transmitting antenna, a current will be induced in this object [1, 2]. This current will radiate and if kP is small, then this will result in a perturbation of the antenna far-field. This effect can in some cases be useful in antenna design. One such example is the Yagi-Uda antenna where currents are induced in parasitic elements (directors and reflectors) which are placed strategically such that the radiated field has an improved directivity [2]. Due to this effect, it is important to distinguish between the far-fields which are perturbed by the presence of the other antenna and the far-fields which are not perturbed by the presence of the other antenna when calculating the dot product in the coupling integral (2.9). In this thesis, these far-fields will be referred to as *perturbed* and *unperturbed* far-fields respectively. The perturbation of the far-fields is expected to increase as kP decreases. It can in some cases be reasonable to use the unperturbed far-fields to calculate the mutual coupling, particularly for large kP and for electrically small or medium-sized antennas. In [17], the unperturbed far-fields were used for medium-sized antennas for $P > 0.2\lambda$.

Chapter 3

Calculating the coupling integral using analytical far-fields

In this chapter, we will see that the method described in the previous chapter yields the correct results for some simple antenna configurations. We start by considering antennas with well-known analytical far-fields where it is easy to calculate the dot product in the coupling integral by using $\boldsymbol{f}_{\mathrm{r}}(-\boldsymbol{k}) = \boldsymbol{f}_{\mathrm{r}}(\pi - \theta, \pi + \phi)$ according to (2.42). Dipole antennas are treated in Section 3.1 and circular aperture antennas are considered in Section 3.2.

3.1 Half-wavelength dipole antennas

3.1.1 Electric far-field of an arbitrarily oriented dipole antenna

The electric far-field of a half-wavelength dipole can be found in the literature for the special cases where the dipole is oriented along the z-axis [2], and along the y-axis [17]. In this section, the electric far-field of a half-wavelength dipole oriented in the general direction $\hat{\boldsymbol{n}}$ is derived by analogy with [2]. Some inspiration for this calculation has been taken from the lecture notes in the introductory course on electromagnetic theory at KTH [30]. Assuming that the dipole has the length $h = \lambda/2$ and infinitesimal radius, the electric field can be calculated as a weighted integral over the line current I along the axis defined by $\hat{\boldsymbol{n}}$ [1,2,30]:

$$d\boldsymbol{E}(\boldsymbol{r}, t) = \frac{\mu_0}{4\pi r}\hat{\boldsymbol{r}} \times (\hat{\boldsymbol{r}} \times \hat{\boldsymbol{n}}) \frac{\partial}{\partial t} I\left(\xi', t - \frac{|\boldsymbol{r} - \boldsymbol{r}'|}{c}\right) d\xi' \tag{3.1}$$

where $\boldsymbol{r}' = \xi'\hat{\boldsymbol{n}}$ is the variable of integration along the axis defined by the orientation $\hat{\boldsymbol{n}}$. We assume the complex line current

$$I\left(\xi', t - \frac{|\boldsymbol{r} - \boldsymbol{r}'|}{c}\right) = I_0 \sin\left(\frac{2\pi}{\lambda}\left(\frac{h}{2} - |\xi'|\right)\right) \exp\left(j\omega\left(t - \frac{|\boldsymbol{r} - \boldsymbol{r}'|}{c}\right)\right) \quad (3.2)$$

where $\xi' \in [-h/2, h/2]$ and the harmonic time-dependence $e^{j\omega t}$ is assumed. The current density is assumed to be zero outside the interval $[-h/2, h/2]$ on the axis defined by $\hat{\boldsymbol{n}}$. Omitting the harmonic time-dependence as usual, the far-field can now be calculated:

$$\begin{aligned}
\boldsymbol{E}(\boldsymbol{r}) &\approx j\omega\frac{\mu_0 I_0}{4\pi r}\hat{\boldsymbol{r}} \\
&\quad \times (\hat{\boldsymbol{r}} \times \hat{\boldsymbol{n}}) \int_{-h/2}^{h/2} \sin\left(\frac{2\pi}{\lambda}\left(\frac{h}{2} - |\xi'|\right)\right) \exp\left(j\omega\left(-\frac{r}{c} + \frac{\xi'}{c}\hat{\boldsymbol{n}} \cdot \hat{\boldsymbol{r}}\right)\right) d\xi' \\
&= j\omega\frac{\mu_0 I_0}{4\pi r} e^{-jkr}\hat{\boldsymbol{r}} \times (\hat{\boldsymbol{r}} \times \hat{\boldsymbol{n}}) \int_{-h/2}^{h/2} \sin\left(\frac{2\pi}{\lambda}\left(\frac{h}{2} - |\xi'|\right)\right) e^{jk\xi'\hat{\boldsymbol{n}}\cdot\hat{\boldsymbol{r}}} d\xi' \\
&= j\omega\frac{\mu_0 I_0}{4\pi r} e^{-jkr}\hat{\boldsymbol{r}} \times (\hat{\boldsymbol{r}} \times \hat{\boldsymbol{n}})\, Q(\boldsymbol{r})
\end{aligned} \quad (3.3)$$

where the far-field approximation

$$t - \frac{|\boldsymbol{r} - \boldsymbol{r}'|}{c} \approx t - \frac{r}{c} + \frac{\xi'}{c}\hat{\boldsymbol{n}} \cdot \hat{\boldsymbol{r}} \quad (3.4)$$

has been used. Using Euler's formula, we note that the imaginary part of the integrand is odd in ξ' and will thus not contribute to the integral. Hence, the remaining part of the integral is:

$$Q(\boldsymbol{r}) = \frac{2}{k}\frac{\cos\left(\frac{\pi}{2}\hat{\boldsymbol{n}} \cdot \hat{\boldsymbol{r}}\right)}{1 - (\hat{\boldsymbol{n}} \cdot \hat{\boldsymbol{r}})^2} \quad (3.5)$$

The electric far-field of a half-wavelength antenna oriented in the direction $\hat{\boldsymbol{n}}$ is thus

$$\boldsymbol{E}(\boldsymbol{r}) = jc\frac{\mu_0 I_0}{2\pi r} e^{-jkr}\hat{\boldsymbol{r}} \times (\hat{\boldsymbol{r}} \times \hat{\boldsymbol{n}})\, \frac{\cos\left(\frac{\pi}{2}\hat{\boldsymbol{n}} \cdot \hat{\boldsymbol{r}}\right)}{1 - (\hat{\boldsymbol{n}} \cdot \hat{\boldsymbol{r}})^2} \quad (3.6)$$

where we note that ω/k equals the phase velocity c for every plane wave. For $\hat{\boldsymbol{n}} = \hat{\boldsymbol{z}}$ and $\hat{\boldsymbol{n}} = \hat{\boldsymbol{y}}$ we have $\hat{\boldsymbol{n}} \cdot \hat{\boldsymbol{r}} = \cos\theta$ and $\sin\theta\sin\phi$ respectively and the result (3.6) can be simplified to the expressions found in [2] and [17]. By normalizing the far-field we find

$$\boldsymbol{f}(\hat{\boldsymbol{r}}) = \frac{1\ \mathrm{V}}{V_0}\hat{\boldsymbol{r}} \times (\hat{\boldsymbol{r}} \times \hat{\boldsymbol{n}})\, \frac{\cos\left(\frac{\pi}{2}\hat{\boldsymbol{n}} \cdot \hat{\boldsymbol{r}}\right)}{1 - (\hat{\boldsymbol{n}} \cdot \hat{\boldsymbol{r}})^2} \quad (3.7)$$

By substituting $e^{-i\omega t}$ for $e^{j\omega t}$ in the derivation above, it is readily shown that (3.7) is valid for both choices of time dependence. The normalized directivity of a half-wavelength dipole oriented along the direction $\hat{\boldsymbol{n}} = (\hat{\boldsymbol{x}} + \hat{\boldsymbol{y}})/\sqrt{2}$ is plotted in Fig. 3.1.

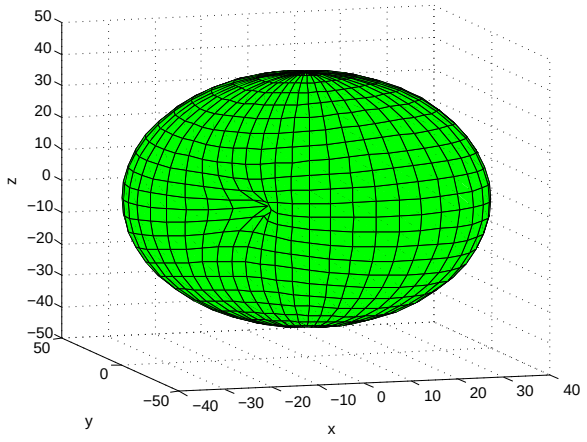

Figure 3.1: Normalized directivity of a half-wavelength dipole oriented in the direction $\hat{\boldsymbol{n}} = (\hat{\boldsymbol{x}} + \hat{\boldsymbol{y}})/\sqrt{2}$.

3.1.2 Mutual coupling between arbitrarily oriented half-wavelength dipoles

The electric far-field of an arbitrarily oriented half-wavelength dipole antenna was presented in the previous section. It is thus possible to calculate the mutual coupling between two arbitrarily oriented dipole antennas by evaluating the coupling integral (2.9). The first step is to calculate the dot product $\boldsymbol{f}_{\mathrm{r}}(-\hat{\boldsymbol{r}}) \cdot \boldsymbol{f}_{\mathrm{t}}(\hat{\boldsymbol{r}})$ where the dipole orientations are given by $\hat{\boldsymbol{n}}_{\mathrm{r}}$ and $\hat{\boldsymbol{n}}_{\mathrm{t}}$ respectively.

Real dipole antennas always have a small amount of unwanted cross-polarization. This results in a small mutual coupling between perpendicular dipoles (where $\hat{\boldsymbol{n}}_{\mathrm{r}} \cdot \hat{\boldsymbol{n}}_{\mathrm{t}} = 0$). This unwanted cross-polarization is not present in (3.6) and the coupling between two perpendicular dipoles calculated using (3.6) should therefore be identically zero. Note that there are several possible $\boldsymbol{f}_{\mathrm{r}}(-\hat{\boldsymbol{r}}) \cdot \boldsymbol{f}_{\mathrm{t}}(\hat{\boldsymbol{r}})$ for which the coupling integral (2.9) equals zero. One obvious case is $\boldsymbol{f}_{\mathrm{r}}(-\hat{\boldsymbol{r}}) \cdot \boldsymbol{f}_{\mathrm{t}}(\hat{\boldsymbol{r}}) = 0$ for all $\hat{\boldsymbol{r}}$. Another case is when there is a symmetry in the dot product such that

$$t(\theta) \equiv \int_0^{2\pi} \boldsymbol{f}_{\mathrm{r}}(-\hat{\boldsymbol{r}}) \cdot \boldsymbol{f}_{\mathrm{t}}(\hat{\boldsymbol{r}}) d\phi \tag{3.8}$$

is zero. The function $t(\theta)$ was introduced by Yaghjian in [7] and it will be used also in Section 4.1.

In order to implement the dot product $\boldsymbol{f}_{\mathrm{r}}(-\hat{\boldsymbol{r}}) \cdot \boldsymbol{f}_{\mathrm{t}}(\hat{\boldsymbol{r}})$ in a computer program, it is useful to expand the vector triple product using the $\epsilon - \delta$ identity, which describes the relation between the alternating tensor ϵ_{ijk} and the Kronecker delta δ_{ij} [1, 26] :

$$\epsilon_{ijk}\epsilon_{klm} = \delta_{il}\delta_{jm} - \delta_{im}\delta_{jl} \Rightarrow \boldsymbol{a} \times (\boldsymbol{b} \times \boldsymbol{c}) = (\boldsymbol{a} \cdot \boldsymbol{c})\boldsymbol{b} - (\boldsymbol{a} \cdot \boldsymbol{b})\boldsymbol{c} \tag{3.9}$$

$$\Rightarrow \hat{\boldsymbol{r}} \times (\hat{\boldsymbol{r}} \times \hat{\boldsymbol{n}}) = (\hat{\boldsymbol{r}} \cdot \hat{\boldsymbol{n}})\hat{\boldsymbol{r}} - \hat{\boldsymbol{n}} \tag{3.10}$$

Hence,

$$\begin{aligned}
\boldsymbol{f}_{\mathrm{r}}(\boldsymbol{r}_{\mathrm{r}}) \cdot \boldsymbol{f}_{\mathrm{t}}(\boldsymbol{r}_{\mathrm{t}}) &= \hat{\boldsymbol{r}}_{\mathrm{r}} \times (\hat{\boldsymbol{r}}_{\mathrm{r}} \times \hat{\boldsymbol{n}}_{\mathrm{r}}) \frac{\cos\left(\frac{\pi}{2}\hat{\boldsymbol{n}}_{\mathrm{r}} \cdot \hat{\boldsymbol{r}}_{\mathrm{r}}\right)}{1-(\hat{\boldsymbol{n}}_{\mathrm{r}} \cdot \hat{\boldsymbol{r}}_{\mathrm{r}})^2} \cdot \left[\hat{\boldsymbol{r}}_{\mathrm{t}} \times (\hat{\boldsymbol{r}}_{\mathrm{t}} \times \hat{\boldsymbol{n}}_{\mathrm{t}}) \frac{\cos\left(\frac{\pi}{2}\hat{\boldsymbol{n}}_{\mathrm{t}} \cdot \hat{\boldsymbol{r}}_{2}\right)}{1-(\hat{\boldsymbol{n}}_{\mathrm{t}} \cdot \hat{\boldsymbol{r}}_{\mathrm{t}})^2}\right] \\
&= \left[\frac{\cos\left(\frac{\pi}{2}\hat{\boldsymbol{n}}_{\mathrm{r}} \cdot \hat{\boldsymbol{r}}_{\mathrm{r}}\right)}{1-(\hat{\boldsymbol{n}}_{\mathrm{r}} \cdot \hat{\boldsymbol{r}}_{\mathrm{r}})^2}\right]\left[\frac{\cos\left(\frac{\pi}{2}\hat{\boldsymbol{n}}_{\mathrm{t}} \cdot \hat{\boldsymbol{r}}_{\mathrm{t}}\right)}{1-(\hat{\boldsymbol{n}}_{\mathrm{t}} \cdot \hat{\boldsymbol{r}}_{\mathrm{t}})^2}\right]((\hat{\boldsymbol{r}}_{\mathrm{r}} \cdot \hat{\boldsymbol{n}}_{\mathrm{r}})\hat{\boldsymbol{r}}_{\mathrm{r}} - \hat{\boldsymbol{n}}_{\mathrm{r}}) \\
&\quad \cdot ((\hat{\boldsymbol{r}}_{\mathrm{t}} \cdot \hat{\boldsymbol{n}}_{\mathrm{t}})\hat{\boldsymbol{r}}_{\mathrm{t}} - \hat{\boldsymbol{n}}_{\mathrm{t}}) \\
&= \left[\frac{\cos\left(\frac{\pi}{2}\hat{\boldsymbol{n}}_{\mathrm{r}} \cdot \hat{\boldsymbol{r}}_{\mathrm{r}}\right)}{1-(\hat{\boldsymbol{n}}_{\mathrm{r}} \cdot \hat{\boldsymbol{r}}_{\mathrm{r}})^2}\right]\left[\frac{\cos\left(\frac{\pi}{2}\hat{\boldsymbol{n}}_{\mathrm{t}} \cdot \hat{\boldsymbol{r}}_{\mathrm{t}}\right)}{1-(\hat{\boldsymbol{n}}_{\mathrm{t}} \cdot \hat{\boldsymbol{r}}_{\mathrm{t}})^2}\right] \\
&\quad ((\hat{\boldsymbol{r}}_{\mathrm{r}} \cdot \hat{\boldsymbol{n}}_{\mathrm{r}})(\hat{\boldsymbol{r}}_{\mathrm{t}} \cdot \hat{\boldsymbol{n}}_{\mathrm{t}})(\hat{\boldsymbol{r}}_{\mathrm{r}} \cdot \hat{\boldsymbol{r}}_{\mathrm{t}}) - (\hat{\boldsymbol{r}}_{\mathrm{r}} \cdot \hat{\boldsymbol{n}}_{\mathrm{r}})(\hat{\boldsymbol{r}}_{\mathrm{r}} \cdot \hat{\boldsymbol{n}}_{\mathrm{t}}) - (\hat{\boldsymbol{r}}_{\mathrm{t}} \cdot \hat{\boldsymbol{n}}_{\mathrm{t}})(\hat{\boldsymbol{r}}_{\mathrm{t}} \cdot \hat{\boldsymbol{n}}_{\mathrm{r}}) + \hat{\boldsymbol{n}}_{\mathrm{r}} \cdot \hat{\boldsymbol{n}}_{\mathrm{t}})
\end{aligned} \tag{3.11}$$

It is readily shown that $\hat{\boldsymbol{r}} = -\hat{\boldsymbol{r}}_{\mathrm{r}} = \hat{\boldsymbol{r}}_{\mathrm{t}}$ and $\hat{\boldsymbol{n}}_{\mathrm{r}} \cdot \hat{\boldsymbol{n}}_{\mathrm{t}} = 0$ results in $t(\theta) = 0$. This can be seen in the two special cases in Fig. 3.2. Hence, the mutual coupling is identically zero for perpendicularly oriented dipoles. This is an important result since it shows consistency of the coupling integral (2.9) with our previous knowledge of the mutual coupling between linearly polarized antennas with perpendicular polarization.

Finally, the mutual coupling between two dipoles oriented along the y-axis and separated a distance d along the z-axis is calculated. The dot product (3.11) may be simplified to:

$$\boldsymbol{f}_{\mathrm{r}}(-\hat{\boldsymbol{r}}) \cdot \boldsymbol{f}_{\mathrm{t}}(\hat{\boldsymbol{r}}) = \left[\frac{\cos(\frac{\pi}{2}\sin\theta\sin\phi)}{1-(\sin\theta\sin\phi)^2}\right]^2 (1-\sin^2\theta\sin^2\phi) \tag{3.12}$$

The mutual coupling between two antennas was calculated as function of separation distance using the time domain solver in CST for 10 GHz. The results from simulation, series expansion (2.33) and Friis transmission equation is found in Fig. 3.3. Since we have not taken into account any perturbation of the fields due to the presence of the second antenna when calculating (3.12), the unperturbed far-fields are used. V_0 was calculated according to (2.16) to take the antenna losses into account. According to (2.35) we expect good agreement for $d > 0.5\lambda$ which agrees well with Fig. 3.3. Furthermore, it is clear that the asymptotic behavior of the coupling integral also agrees well with Friis transmission equation (2.4).

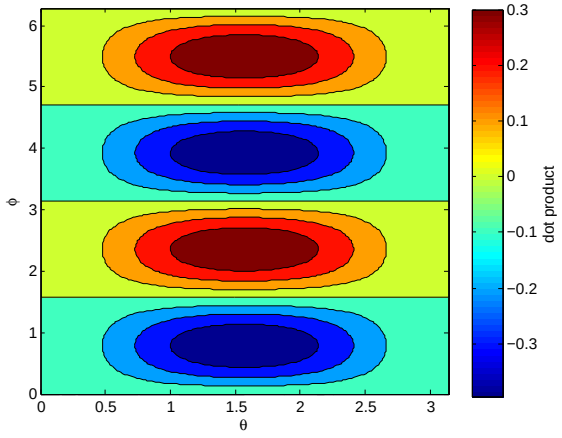

(a)

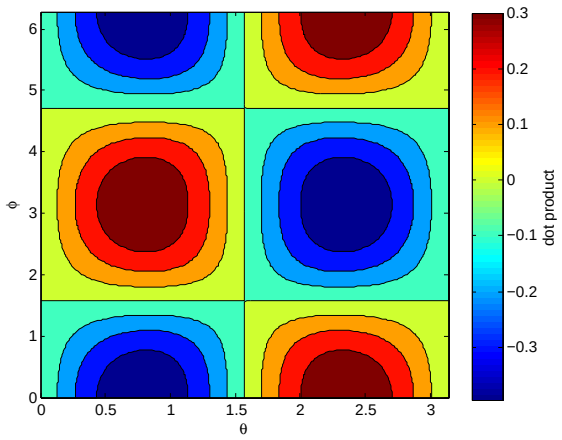

(b)

Figure 3.2: Normalized dot product $\boldsymbol{f}_{\mathrm{r}}(-\hat{\boldsymbol{r}}) \cdot \boldsymbol{f}_{\mathrm{t}}(\hat{\boldsymbol{r}})$ for (a) $\hat{\boldsymbol{n}}_{\mathrm{r}} = \hat{\boldsymbol{x}}$ and $\hat{\boldsymbol{n}}_{\mathrm{t}} = \hat{\boldsymbol{y}}$ and (b) $\hat{\boldsymbol{n}}_{\mathrm{r}} = \hat{\boldsymbol{x}}$ and $\hat{\boldsymbol{n}}_{\mathrm{t}} = \hat{\boldsymbol{z}}$. These dot products have a symmetry such that $t(\theta) = 0$.

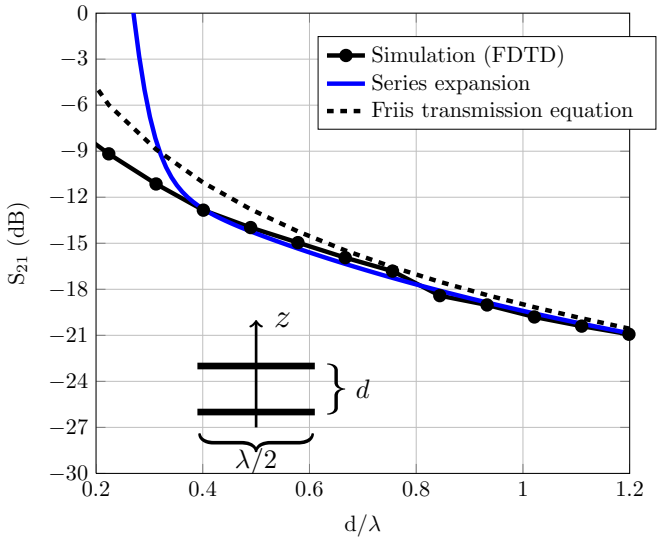

Figure 3.3: Mutual coupling between two half-wavelength dipoles which are parallel and separated along the z-axis according to the illustration.

3.2 Electrically large circular aperture antennas

The mutual coupling between two electrically large circular aperture antennas was calculated using both the series expansion (2.39) and the non-singular coupling integral (2.41). The results agree well with results found in the literature [7, 20].

A circular aperture with radius ρ located in an infinite grounded plane in $z = 0$ illuminated by the uniform aperture field $\boldsymbol{E}_a(\boldsymbol{r}) = E_0\hat{\boldsymbol{y}}$ has the following far-field [2]:

$$\boldsymbol{E}(\boldsymbol{r}) = -\frac{k\rho^2 E_0 e^{-jkr}}{r}\left(\hat{\boldsymbol{\theta}}\sin\phi + \hat{\boldsymbol{\phi}}\cos\theta\cos\phi\right)\frac{J_1(Z)}{Z} \tag{3.13}$$

where

$$Z \equiv k\rho\sin\theta \tag{3.14}$$

and J_1 is the first-order Bessel function. The normalized far-field is thus given by:

$$\boldsymbol{f}(\theta,\phi) = \frac{1\ \mathrm{V}}{V_0}\frac{J_1(Z)}{Z}\left(\hat{\boldsymbol{y}}\cos\theta - \hat{\boldsymbol{z}}\sin\theta\sin\phi\right). \tag{3.15}$$

The apertures are assumed to be lossless and perfectly matched. V_0 is therefore calculated using (2.17). The antennas have the same radius and are oriented such that $\boldsymbol{f}_{\mathrm{r}}(-\hat{\boldsymbol{r}}) = \boldsymbol{f}_{\mathrm{t}}(\hat{\boldsymbol{r}}) = \boldsymbol{f}(\hat{\boldsymbol{r}})$. Noting that the far-fields are real-valued, it is possible to calculate the dot product in the coupling integral according

to $\boldsymbol{f}_{\mathrm{r}}(-\hat{\boldsymbol{r}}) \cdot \boldsymbol{f}_{\mathrm{t}}(\hat{\boldsymbol{r}}) = |\boldsymbol{f}(\hat{\boldsymbol{r}})|^2 = D(\hat{\boldsymbol{r}})/(4\pi)$ where D is the directivity of the aperture. The time-convention $e^{j\omega t}$ was used when deriving (3.13) and the coupling integral should therefore be calculated using (2.39) or (2.41).

The mutual coupling between two electrically large circular apertures with diameter $2\rho = 50\lambda$ was calculated as function of the separation distance d for the setup depicted in Fig. 2.3. The problem was first solved using the series expansion (2.39). Note that the Legendre polynomials have the following property [29]:

$$\mathrm{P}_n(-x) = (-1)^n \mathrm{P}_n(x) \tag{3.16}$$

i.e. $P_n(\cos\theta)$ is even (odd) around $\theta = \pi/2$ if n is even (odd). $D(\theta,\phi) = D(-\theta,\phi)$ for this antenna, and consequently $B_{2n+1} = 0$. The magnitude of the nonzero coefficients in the expansion are presented in Fig. 3.5. The result from the expansion is presented in Fig. 3.4. According to (2.5), reasonable agreement with Friis transmission equation is expected for $d/\lambda > 2(D/\lambda)^2 = 5000$. On the other hand, the expansion (2.33) is according to (2.35) valid for $d/\lambda > (\rho_{\mathrm{r}} + \rho_{\mathrm{t}})/\lambda = 50$. The results in Fig. 3.4 are in excellent agreement with [7] and [20]. Furthermore, the number of modes required in this expansion is in good agreement with (2.37).

The same problem was thereafter solved by numerical integration of the NSCI (2.41). The agreement between the series expansion (2.39) and the NSCI (2.41) is excellent (Fig. 3.6). The integrals (2.41) and (2.38) (or equivalently (2.9)) are computationally expensive for large antenna separations due to the rapidly varying exponential factor in the integrand. It could therefore be advantageous to use the series expansion (2.39) for large antenna separations. Note however that a large number of terms are needed in this series expansion according to (2.37) if the antennas are electrically large. For shorter antenna separations, it is therefore faster to use the NSCI (2.41). Furthermore, the NSCI (2.41) gives reasonable results for $d < r_0$ where the series expansion does not converge according to (2.35).

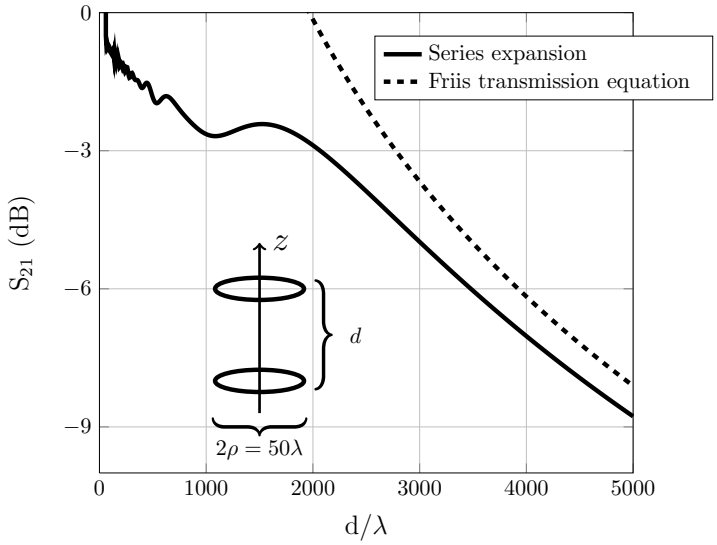

Figure 3.4: Mutual coupling between two circular apertures with diameter $2\rho = 50\lambda$ in the configuration depicted in Fig. 2.3 as function of separation distance d.

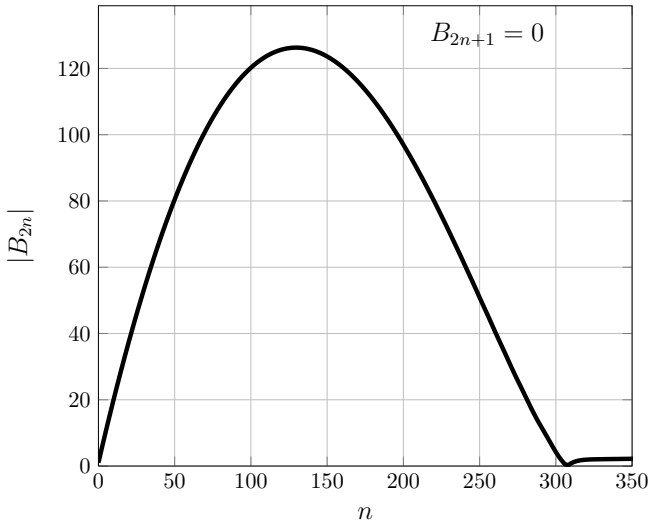

Figure 3.5: Magnitude of the coefficients in the expansion (2.39) corresponding to the results in Fig. 3.4.

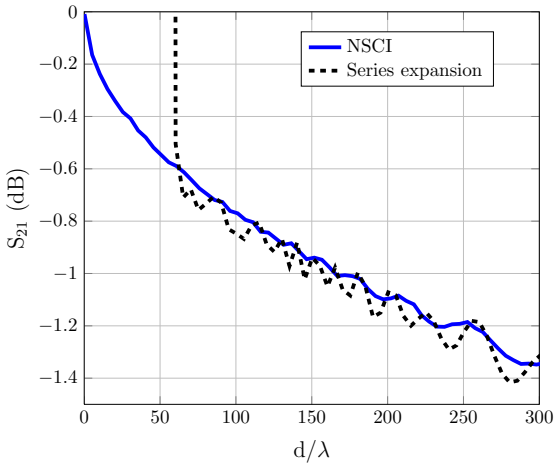

Figure 3.6: Comparison between the NSCI (2.41) and the series expansion (2.39) for small antenna separations.

Chapter 4

Calculating the coupling integral using sampled far-fields

The integrals encountered so far have some common properties. Most importantly, their respective integrands consist of $\boldsymbol{f}_{\mathrm{r}}(-\boldsymbol{k}) \cdot \boldsymbol{f}_{\mathrm{t}}(\boldsymbol{k})$ multiplied by some rapidly varying weight function p. Hence, the integrals are of the type

$$\int g(x)p(x)dx \tag{4.1}$$

where p is varying more rapidly than g in the integration variable(s) x. In this chapter we consider the case where the antenna far-fields are given as a sampled data set with a limited number of samples. According to the sampling theorem [31], a larger number of samples is required in order to correctly sample the integrand gp compared to sampling the relatively slowly varying function g. The number of available samples in g is limited and it could therefore be necessary to interpolate this function in order to achieve the required sample spacing when sampling gp.

This chapter will address the problems of sample spacing, interpolation and efficient numerical integration of integrals of the type (4.1). Finally, the non-singular coupling integral (2.41) and the series expansion (2.39) will be calculated for some specific antenna types. Horn, spiral and helical antennas will be considered. The electric far-fields of these antennas will be calculated using CST Microwave studio and the results from calculating the coupling integral with (2.39) and (2.41) will be compared with the mutual coupling calculated using CST. More information about CST is found in Section 4.2. The unperturbed far-fields (see Section 2.6) will be used throughout this Chapter. Based on these results, a step-by-step procedure for calculating the mutual coupling between two arbitrary antennas designed in CST has been developed. This procedure is described in Section 4.7.

4.1 A hybrid method for efficient double integration

Using the terminology of [32], integrals of the type (4.1) belong to a class of integrals with the self-explanatory name "difficult integrals". These integrals are difficult from a numerical point of view due to the rapidly varying integrand. Initially, a two-dimensional trapezoidal rule was used to calculate the coefficients in the expansion (2.39) for a predetermined sample spacing. For this purpose, a Matlab function named `trapz2D` was developed. It was later found that an integration with better quality could be achieved if the sampled dot product is interpolated and an adaptive integrator such Matlab's built-in `dblquad` or `quad2d` is used. `quad2d` is sufficient for most practical problems, but it is still of interest to investigate if there are any faster methods available. One such method is presented in this section.

The integration over ϕ is the same for all coefficients (2.40) in the expansion (2.39). Similarly for (2.41), only the integration over θ needs to be repeated when changing d while $R = 0$. We therefore start by calculating the following integral:

$$t(\theta) = \int_0^{2\pi} \boldsymbol{f}_{\mathrm{r}}(-\boldsymbol{r}) \cdot \boldsymbol{f}_{\mathrm{t}}(\boldsymbol{r}) d\phi. \tag{4.2}$$

After calculating $t(\theta)$, both (2.40) and (2.41) may be expressed as integrals over only one variable (θ). Since the integration over ϕ is only done once, a shorter computational time will be required when evaluating several integrals.

The integration (4.2) is relatively simple from a numerical point of view for most antennas and this integration can therefore be performed using one of Matlab's built-in integrators e.g. `quad` or `quadl`. The remaining integration over θ is challenging due to the rapidly oscillating integrand, particularly for large d in (2.41) and large n in (2.34). In these cases, a special method for integration of rapidly oscillating functions called `quade` [32] has been used.

The coefficients (2.40) are independent and can thus be computed in parallel. Similarly, it is possible to parallelize the evaluation of (2.41) for several antenna separations d. This reduces the computational time on a computer with several cores. In Matlab, this can be achieved by replacing the conventional `for`-loop with a the parallel loop `parfor` [33].

4.2 Notes on CST Microwave Studio

The far-fields used when evaluating the dot-product $\boldsymbol{f}_{\mathrm{r}}(-\boldsymbol{k}) \cdot \boldsymbol{f}_{\mathrm{t}}(\boldsymbol{k})$ are, with the exception of the previously considered analytical fields, calculated using the commercial software CST Microwave Studio [21] in this thesis. The main advantage of using this type of software is that it also can be used to calculate the mutual coupling between the considered antennas. The far-fields calculated by CST are used as synthetic data and the mutual coupling calculated with CST

will be used as a reference when evaluating the coupling program developed in this thesis.

The aim of this section is to describe which settings in CST are appropriate to use for the type of problems solved during this thesis. If inappropriate settings are used, the required computational time can become excessive and in the worst case, the solutions can be inaccurate. It is therefore a good habit to check that the results do not change notably when changing the solver parameters. This kind of sensitivity analysis can be used to identify unreliable solutions.

The time-domain solver (FDTD) is very well suited for a large class of problems. The main advantage in calculating scattering parameters using FDTD is that the scattering parameters are found as a function of frequency whereas most other methods only solve for one frequency sample at a time. There are however some disadvantages in using FDTD to calculate the mutual coupling between antennas if the antenna separation is large. Firstly, the computational domain and consequently the number of mesh elements increases as the antenna separation in increases. The distance between the antennas and the bounding Perfectly Matched Layer (PML) must also be chosen with care when using FDTD. The integral equation solver does not suffer from these problems and it has therefore been used for the majority of problems in this thesis.

The integral equation solver in CST can be set to use either the Method of Moments (MoM) or the Multi Level Fast Multipole Method (MLFMM). An important setting for the integral equation solver is the solver order. The first order is fast and sufficient for a large class of problems. The second order is more accurate and has therefore been used when the results found using the first order solver were not accurate enough.

Far-fields calculated by CST can be exported to ASCII files using the option "Save as source". An electric far-field exported from CST using this option are hereafter referred to as $\boldsymbol{E}_{CST}$ and by default, the following normalization is used [21]:

$$G(\boldsymbol{r}) = \frac{4\pi}{Z_0}|\boldsymbol{E}_{CST}(\boldsymbol{r})|^2/(1\ \mathrm{W/m^2}) \tag{4.3}$$

where $Z_0 \approx 377\ \Omega$ is the impedance of free space. It should be noted that $\boldsymbol{E}_{CST}(\boldsymbol{r})$ is defined such that impedance mismatch and thermal losses have been taken into account. From (2.16) we consequently find:

$$\boldsymbol{f}(\boldsymbol{r}) = \frac{1}{\sqrt{Z_0}\sqrt{1\ \mathrm{W/m^2}}}\boldsymbol{E}_{CST}(\boldsymbol{r}) \tag{4.4}$$

There is a built-in lower limit in the angular sample spacing when exporting the far-fields from CST. This lower limit is set to 0.25°. This is not sufficient for certain applications, particularly for electrically large antennas. Hence, a Visual Basic macro was developed in order to export the far-field for smaller sample spacings. A Matlab function was developed in order to import far-fields stored in the ASCII files produced using this macro. See Appendix A for a complete list of source code.

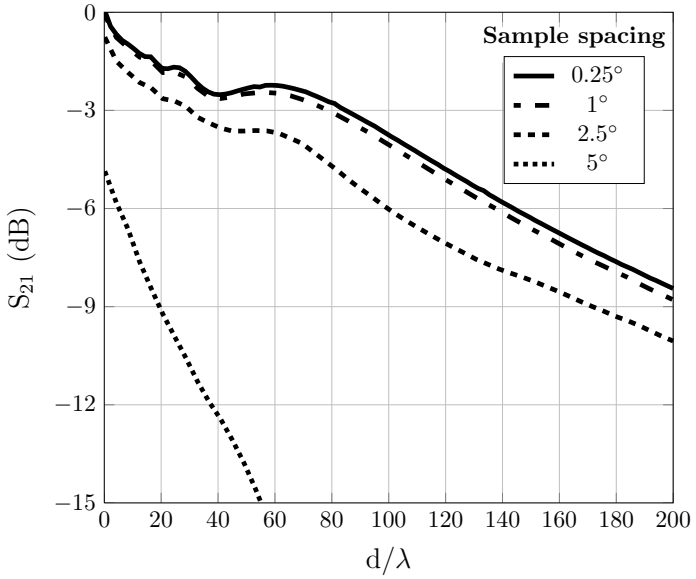

Figure 4.1: Mutual coupling between two circular apertures with diameter $2\rho = 10\lambda$ calculated using the non-singular coupling integral (2.41) with far-fields sampled with different sample spacings.

4.3 Sampling of far-fields

In this section we develop a guideline for sampling of far-fields by presenting a simple numerical experiment. The mutual coupling between two circular aperture antennas with the diameter $2\rho = 10\lambda$ was calculated as function of the separation distance d using the non-singular coupling integral (2.41). The electric far-field (3.15) was sampled on a uniform grid with the sample spacings $5°$, $2.5°$, $1°$ and $0.25°$ respectively. The resulting dot product was interpolated using a linear interpolation before evaluating the integral. The results for the different sample spacings are presented in Fig. 4.1. The errors due to sparse sampling are large for sample spacings greater that $1°$. A sample spacing smaller than $1°$ will therefore be used throughout this thesis when sampling far-fields from antennas of this size or smaller. For larger antennas, a finer sample spacing is required.

4.4 Mutual coupling between spiral antennas

In this section, we verify that the non-singular coupling integral (2.41) and the series expansion (2.39) are correct for circularly polarized antennas. Spiral antennas are easily designed to have circular polarization, and they also have other desirable properties such as a large bandwidth and a low cross polarization

[2]. The spiral antenna presented in Fig. 4.2 is well-matched ($S_{11} < -10$ dB) to a 190 Ω feed throughout the interval $2 - 18$ GHz, which is important for several radar applications. An absorbing layer is placed inside the cavity behind the spiral where $z < 0$ and the main lobe is consequently directed in the positive z-direction. The losses in this layer correspond to roughly 3 dB.

If a LHCP antenna is mirrored in the yz-plane, the result is a RHCP antenna according to Fig. 4.2. The effect of the operator B from Section 2.5 is thus to reverse the polarization of the antenna. Since $\hat{\boldsymbol{n}}_{\mathrm{LHCP}} = \hat{\boldsymbol{n}}^*_{\mathrm{RHCP}}$ (see Section 2.1), this is equivalent to taking the complex conjugate of the far-field. In conclusion, we have the following identity:

$$\boldsymbol{f}(-\boldsymbol{k}) = \boldsymbol{f}(A\boldsymbol{k})^*. \tag{4.5}$$

Another spiral antenna is now added to the CST model according to Fig. 4.3. The second antenna is created by making a copy of the transmitting antenna rotated 180° around the x-axis. These antennas have the same polarization and are therefore polarization-matched. The receiving antenna is finally translated a distance d along the z-axis. Hence, the relation between the receiving and transmitting far-fields is given by $\boldsymbol{f}_{\mathrm{r}}(A\boldsymbol{k}) = \boldsymbol{f}_{\mathrm{t}}(\boldsymbol{k})$. Using (4.5), the dot product in the coupling integral may be simplified according to:

$$\boldsymbol{f}_{\mathrm{t}}(\boldsymbol{k}) \cdot \boldsymbol{f}_{\mathrm{r}}(-\boldsymbol{k}) = \boldsymbol{f}_{\mathrm{t}}(\boldsymbol{k}) \cdot \boldsymbol{f}_{\mathrm{r}}(A\boldsymbol{k})^* = \boldsymbol{f}_{\mathrm{t}}(\boldsymbol{k}) \cdot \boldsymbol{f}_{\mathrm{t}}(\boldsymbol{k})^* \equiv \frac{1}{4\pi} G_{\mathrm{t}}(\boldsymbol{k}) \tag{4.6}$$

where we use $AA = \mathrm{I}$ and the normalization (2.16).

As a comparison, we also simulate polarization-mismatched antennas in the same setup. The receiving antenna is in this case created by mirroring the original antenna in the yz-plane, and it is thereafter rotated 180° around the x-axis similarly to the polarization matched case. The relation between the receiver and transmitter far-fields is then $\boldsymbol{f}_{\mathrm{r}}(A\boldsymbol{k}) = \boldsymbol{f}_{\mathrm{t}}(\boldsymbol{k})^*$. The dot product coupling integral may now be simplified to:

$$\boldsymbol{f}_{\mathrm{t}}(\boldsymbol{k}) \cdot \boldsymbol{f}_{\mathrm{r}}(-\boldsymbol{k}) = \boldsymbol{f}_{\mathrm{t}}(\boldsymbol{k}) \cdot \boldsymbol{f}_{\mathrm{r}}(A\boldsymbol{k})^* = \boldsymbol{f}_{\mathrm{t}}(\boldsymbol{k}) \cdot \boldsymbol{f}_{\mathrm{t}}(\boldsymbol{k}) \tag{4.7}$$

In order to evaluate the dot product in the coupling integral we need to export both $\boldsymbol{f}_{\mathrm{t}}(\boldsymbol{k})$ and $\boldsymbol{f}_{\mathrm{r}}(-\boldsymbol{k})$ from the CST model before performing the integration in Matlab. When exporting the far-fields, it will be useful to introduce the local system of coordinates presented in Fig. 2.1. O_{t} and O_{r} are chosen to be in the center of each spiral. The phase shift between these two points is taken into account by the complex exponential in the coupling integral and we should therefore use far-fields which are expressed in their local system of coordinates when calculating the dot product. It is therefore important to note that the distance between the antennas, $\boldsymbol{P}$, is defined as the distance between O_{t} and O_{r}. The far-field of the transmitting antenna is exported in the local system of coordinates which coincides with the global system of coordinates. According to (4.5) we can export $\boldsymbol{f}_{\mathrm{r}}(A\boldsymbol{k})$ from CST and thereafter apply the complex conjugate in Matlab rather than exporting $\boldsymbol{f}_{\mathrm{r}}(-\boldsymbol{k})$ from CST. It should be noted

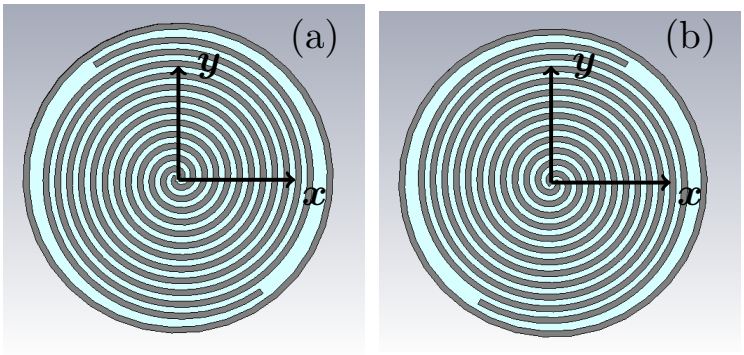

Figure 4.2: Spiral antennas with (a) RHCP (b) LHCP. The system of coordinates is marked in the center of respective figure.

that $\boldsymbol{f}_{\mathrm{r}}(A\boldsymbol{k})$ is the field seen in the local system of coordinates S_{r} when $\boldsymbol{k}$ is expressed in the global system of coordinates.

The diameter of the spiral antenna is $D'/\lambda = 1.7$ for 10 GHz. According to (2.35), the expansion (2.33) is therefore valid for $d > \rho_{\mathrm{r}} + \rho_{\mathrm{t}} = 1.7\lambda$ and according to the rule of thumb (2.5), Friis transmission equation is valid for $d > 5.8\lambda$. Since the unwanted cross-polarization for this antenna is very low, we expect the mutual coupling between polarization-mismatched antennas to be well below the mutual coupling between polarization-matched antennas. The mutual coupling calculated using CST is found in Fig. 4.4 at the center frequency 10 GHz. The unperturbed far-field was sampled on a uniform grid with a sample spacing of 0.5° and the resulting dot product was interpolated before calculating the non-singular coupling integral and the coefficients in the series expansion. An excellent agreement was found between the simulation results and the non-singular coupling integral (2.41) for all separation distances and as expected, the agreement with the series expansion (2.39) is excellent for separation distances $d > 1.7\lambda$. It should be noted that the agreement is better for the polarization matched case than the polarization mismatched case. This can be explained by the fact that the unperturbed far-fields are used and the amount of cross polarization of one antenna can change due to the presence of another antenna located within the near-field.

Finally, we rotate the receiving antenna 30° around the x_{r}-axis, i.e. the axis which is parallel with $\hat{\boldsymbol{x}}$ and passing through O_{r}. Furthermore, we now calculate the mutual coupling as function R_y, i.e. the antenna separation along the y-axis. The configuration is presented in Fig. 4.5 and the polarization-matched case is considered. The far-field of the receiving antenna $\boldsymbol{f}_{\mathrm{r}}(-\boldsymbol{k})$ can be calculated using two different procedures. Using the first method, $\boldsymbol{f}(A\boldsymbol{k})$ is exported from CST in the post processing stage. $\boldsymbol{f}(A\boldsymbol{k})$ is the far-field exported when using the local system of coordinates S_{r}. It is thereafter possible to calculate the dot product $\boldsymbol{f}_{\mathrm{r}}(-\boldsymbol{k}) \cdot \boldsymbol{f}_{\mathrm{t}}(\boldsymbol{k})$ using (4.5). The second method is to also mirror the

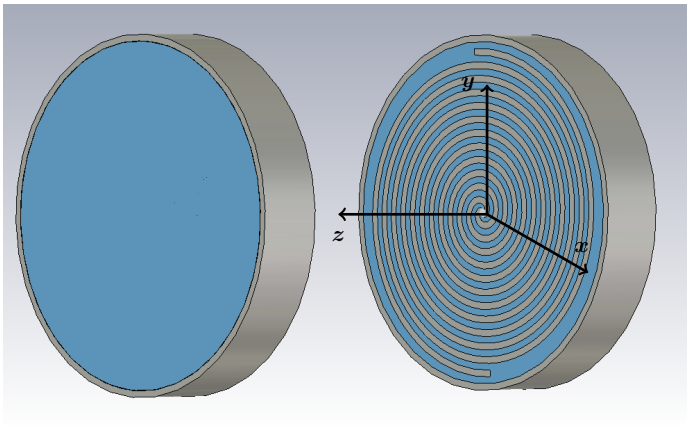

Figure 4.3: Two spiral antennas facing each other in the configuration from Fig. 2.2 with $\boldsymbol{R} = 0$. The system of coordinates is placed according to Fig. 2.2.

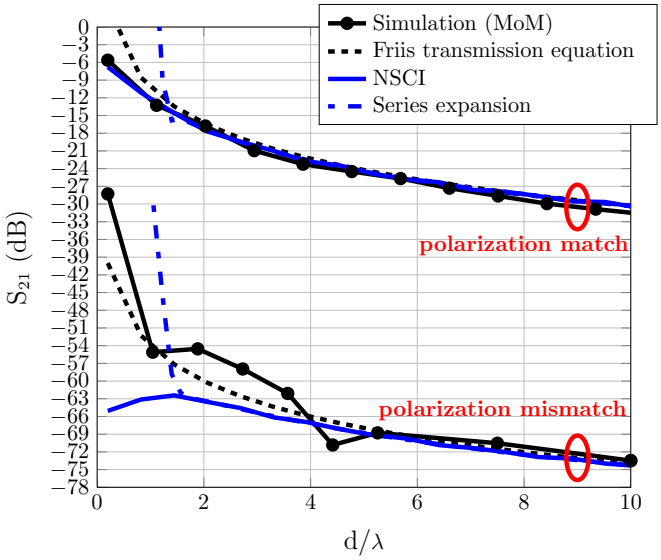

Figure 4.4: Mutual coupling between polarization-matched and polarization-mismatched spiral antennas respectively at the center frequency 10 GHz. The red rings are used to distinguish the curves corresponding to the two different cases under consideration.

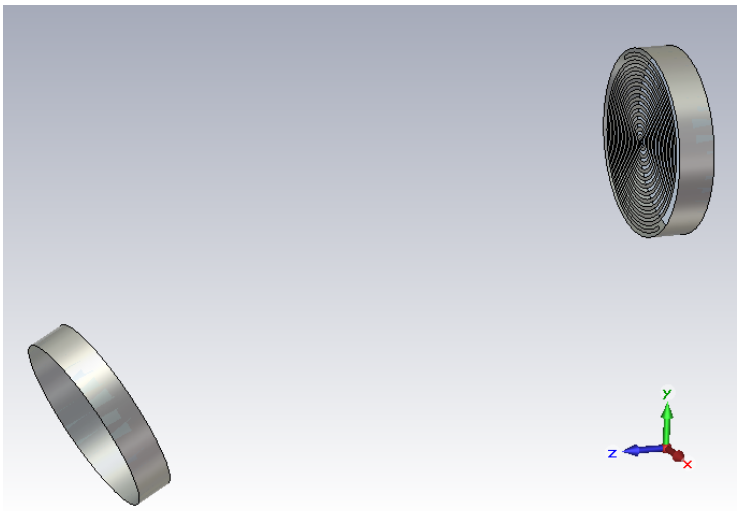

Figure 4.5: Illustration of antenna setup. Comparing with Fig. 4.3, the receiving antenna has been rotated 30° around the x_{r}-axis and moved a distance R_y along the y-axis.

antenna in the yz-plane, i.e. to perform the operation B in CST. The non-singular coupling integral (2.41) was used for both these methods. The results corresponding to $d = 5\lambda$ are presented in Fig. 4.6. As expected, an excellent agreement with the simulation results was found for both methods.

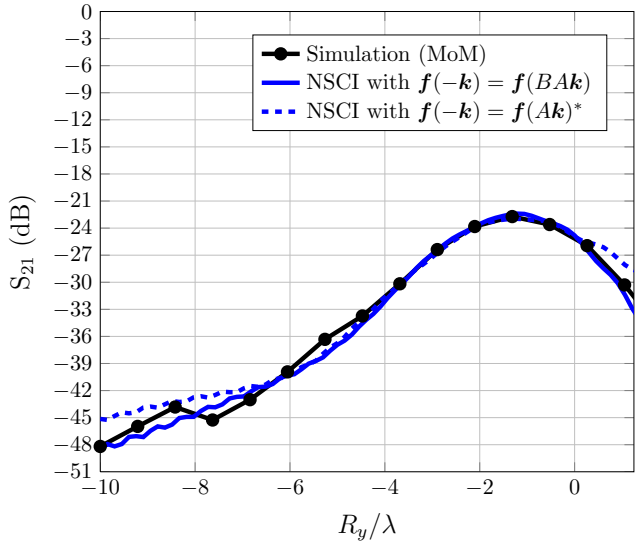

Figure 4.6: Mutual coupling between spiral antennas in the configuration from Fig. 4.5.

4.5 Mutual coupling between horn antennas

In the previous section, we verified that (4.5) is valid for circularly polarized antennas. Since a linear polarization may be decomposed into one LHCP component and one RHCP component [2], this method should be valid also for linearly polarized antennas. Two linearly polarized horn antennas oriented according to Fig. 2.3 are presented in Fig. 4.7. These antennas are polarization-matched and we can therefore use (4.6) when calculating the mutual coupling between them.

The rectangular waveguide feed has a width of 25.4 mm (1 in) and height of 12.7 mm (0.5 in). Hence, the cutoff frequency is for the fundamental mode is $f_{c10} = c/(2 \cdot 0.0254 \text{ m}) = 5.91$ GHz and the lowest cutoff frequency for higher order modes is twice as large, i.e. 11.8 GHz [1, 3]. The antenna operates in the band where only the fundamental mode propagates, i.e. $5.91 - 11.8$ GHz. The mutual coupling (S_{21}) between the antennas is calculated for the frequency 10 GHz using CST. The diameter of the aperture of the horn is $D' = 51$ mm. According to (2.35), the expansion (2.33) is valid for $d > \rho'_\text{r} + \rho'_\text{t} = 1.7\lambda$ and according to the rule of thumb (2.5), Friis transmission equation is valid for $d > 5.8\lambda$. Hence, we can expect reasonable agreement between the simulation in CST and the expansion (2.33) for separation distances greater than 1.7λ.

By performing a parametric sweep in the separation distance d, the relation between S_{21} and d was calculated with CST. The simulation was performed with the direct MoM solver of the second order. d was chosen as the separation

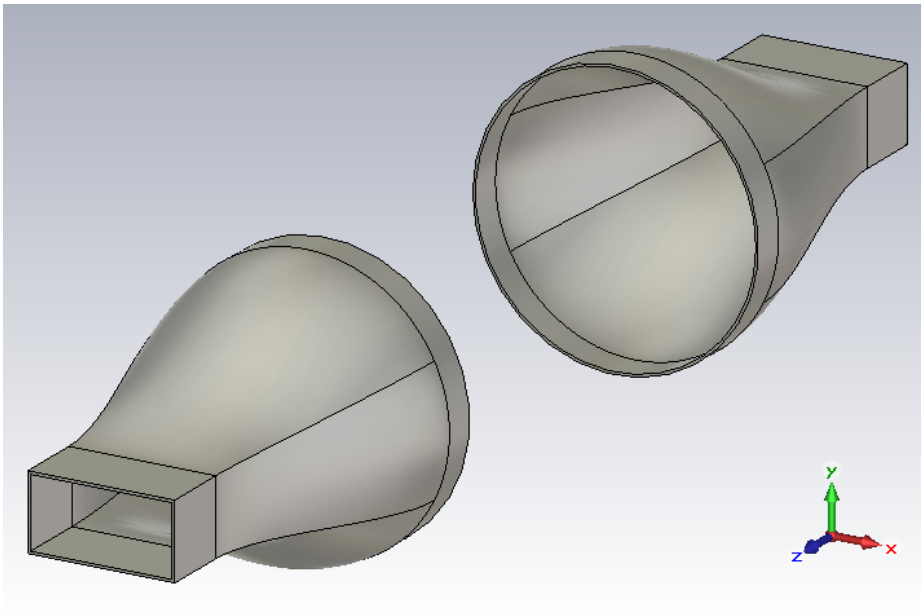

Figure 4.7: Two horn antennas in the setup presented in Fig. 2.3 with $d = 3\lambda$.

distance between the horn apertures. Only the far-field of the transmitter needs to be exported from CST since (4.6) is used to calculate the dot product in the coupling integral. The origin used when calculating the far-fields chosen in the center of the aperture and the z-axis was directed according to Fig. 2.3 and Fig. 4.7. The unperturbed far-field was sampled on a uniform grid with a sample spacing of $0.5°$ and the resulting dot product was interpolated before calculating the non-singular coupling integral and the coefficients in the series expansion. The mutual coupling calculated using CST, the non-singular coupling integral (2.41), the series expansion (2.39) and Friis transmission equation are found in Fig. 4.8. An excellent agreement was found between the simulation results and (2.41) for all separation distances and as expected, the agreement with (2.39) is excellent for separation distances $d > 1.7\lambda$.

4.6 Mutual coupling between two distinct antennas with arbitrary polarization

Finally, we investigate a general case where the receiving and transmitting antennas are of different type. An axial mode helical antenna was designed according to the guidelines in [2]. This circularly polarized antenna was designed to have a significant amount of cross polarization and it is therefore possible to verify that the coupling program correctly takes the cross polarization into account. A system of coordinates is chosen such that the helical antenna may be

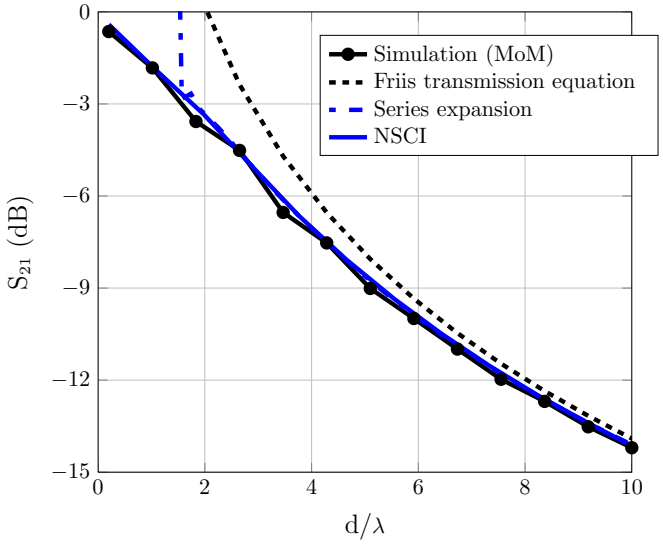

Figure 4.8: Mutual coupling between the horn antennas in Fig. 4.7 as function of separation distance.

interpreted as the transmitting antenna using the notation from Fig. 2.3. The system of coordinates is depicted in Fig. 4.9. It is clear from this figure that there are several ways to choose O_t such that it coincides with the transmitting antenna. Any of these possible choices can be used as long as the same origin is used when calculating the distance between the antennas and calculating the antenna far-fields. The mutual coupling between these antennas are calculated as function of the separation distance d at the frequency 10 GHz and the results are presented in Fig. 4.10. An excellent agreement was found between (2.41) and the simulation results, particularly for the polarization-matched case.

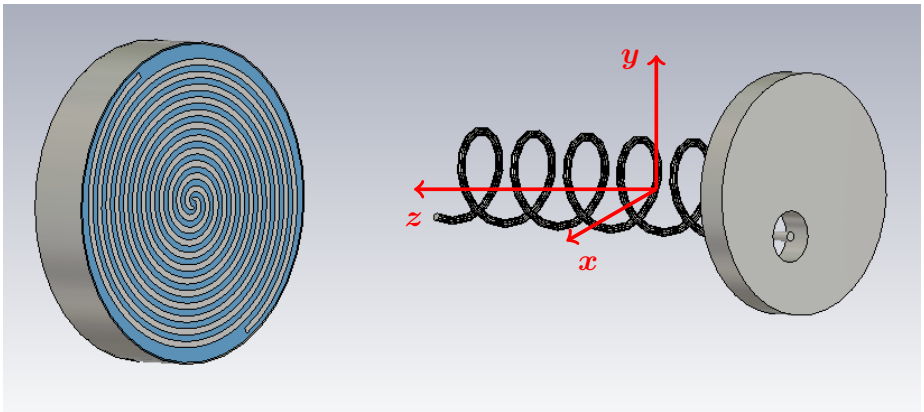

Figure 4.9: A spiral antenna (from Section 4.4) and an axial mode helical antenna (with a coaxial port) with system of coordinates.

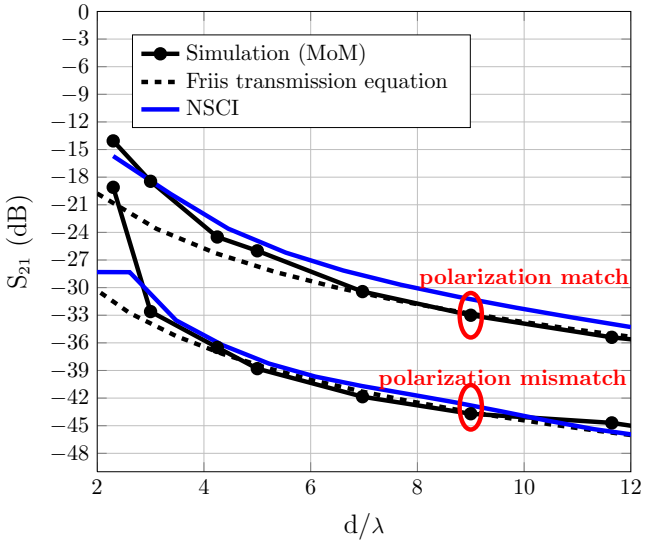

Figure 4.10: Mutual coupling between the antennas in Fig. 4.9 for the polarization matched and polarization mismatched cases respectively. The red rings are used to distinguish the curves corresponding to the two different cases under consideration.

4.7 Overview of the coupling program

The results presented in this chapter have been used to develop a step-by-step procedure for calculating the mutual coupling between two antennas from a CST model. This procedure is described in this section. An overview of the source code is found in Appendix A. The local systems of coordinates S_t and S_r described in Fig. 2.1 are used. The following procedure should be used to calculate the mutual coupling:

i. Export the far-field $\boldsymbol{f}_\mathrm{t}(\boldsymbol{k})$ in the system of coordinates S_t. The macro `exportFF2.mcr` or the CST Graphical User Environment (GUI) with the "Save as source" option can be used to export the far-fields. According to Section 4.3 and the examples considered in this section, 0.5° is an appropriate sample spacing for medium-sized antennas. If there are far-field monitors for several frequencies, then the macro will export the far-field for all these frequencies.

ii. Export $\boldsymbol{f}_\mathrm{r}(A\boldsymbol{k})$ using the same method as in the previous step. The easiest way to export $\boldsymbol{f}_\mathrm{r}(A\boldsymbol{k})$ is to export the receiver's far-field expressed in S_r.

iii. Find the antenna separation $\boldsymbol{P}$ as the distance between O_r and O_t.

iv. Open the coupling program in the Matlab editor. There are several different versions according to Appendix A. Enter the antenna separation(s) P, the file names for the far-field data sets and a filename for the output file.

v. Once the coupling program is finished, it saves the results to a `.mat`-file. The results can finally be plotted by running the post processing script `postprocess.m`.

Chapter 5

Special problems

A step-by-step procedure for calculating the mutual coupling between antennas in the near-field region was developed in the previous chapter. This procedure will be used in this chapter to solve some special problems.

5.1 Mutual coupling as function of frequency

The mutual coupling between antennas has so far in this thesis been calculated as function of the separation distance $\boldsymbol{P}$. In practical applications, it is often more important to know the mutual coupling as function of frequency $f = \omega/(2\pi)$ for some specific antenna separation. As will be seen in this section, it is possible to use the step-by-step procedure developed in the previous chapter to calculate the mutual coupling as function of frequency as well as a function of separation distance. In order to calculate the mutual coupling as function of frequency, we take advantage of the fact that the far-field is a function of frequency. Hence, it is possible to calculate the mutual coupling as function of frequency by running the coupling program for several far-fields corresponding to different frequency samples. When doing this calculation, it is important to remember that electrical distance between the antennas (kd) is also a function of frequency.

As an example, consider a setup where the the receiving antenna in Fig. 4.3 has been replaced by a half-wavelength dipole which has been designed for 10 GHz and oriented along the x-axis. This is an interesting example since there will be a global maximum in the mutual coupling at the resonance of the dipole antenna (10 GHz). The results from simulation and direct integration of the non-singular coupling integral (2.41) for $d = 0.60$ cm (0.20λ for 10 GHz) and $d = 6.0$ cm (2.0λ for 10 GHz) are presented in Fig. 5.1. Clearly, both (2.7) and (2.41) agree well for $d = 6.0$ cm, but (2.41) gives a better estimation than (2.7) for smaller separation distances.

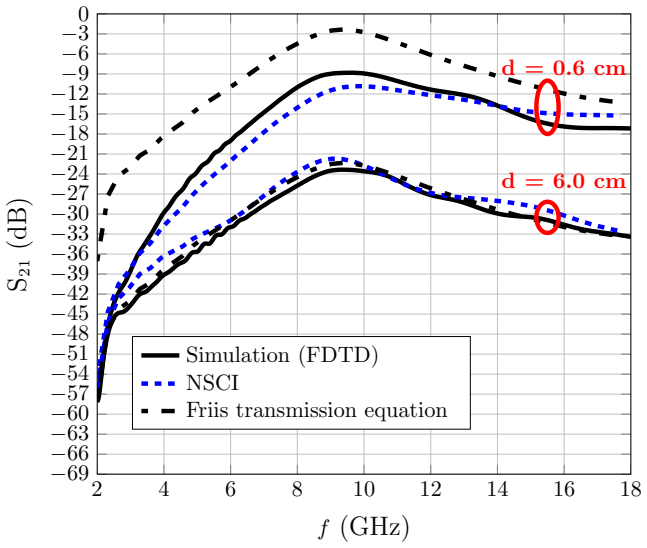

Figure 5.1: Mutual coupling between a spiral antenna and a half-wavelength dipole separated by $d = 0.60$ cm (0.20λ for 10 GHz) and $d = 6.0$ cm (2.0λ for 10 GHz) respectively. The red rings are used to distinguish the curves corresponding to the two different cases under consideration.

5.2 Mutual coupling between antennas on a large conducting object

As a very simple model of two antennas on an aircraft, consider two antennas placed on the electrically large conducting object in Fig. 5.2(a). The two antennas are spiral antennas oriented such that the opening angle 2χ between the conducting planes is 90°. This example represents antenna configurations on an aircraft where the antennas have visual contact. A similar problem for an aircraft could be to calculate the mutual coupling between one antenna installed on the tail of the aircraft and one antenna installed on the wing of the aircraft such that there is visual contact between the antennas. The structure is electrically large which means that a full 3D simulation requires a long computational time.

The coupling integral is derived for two antennas in free space. This scenario can be constructed from the considered geometry by removing a piece of the conducting object according to Fig. 5.2(b). If the antennas have visual contact, this will not notably affect the mutual coupling between the antennas or the antenna far-fields, provided that the change in the geometry is made far enough from respective spiral. With this approximation we can thus find an approximate method for calculating the mutual coupling between the antennas that is significantly faster than performing a full 3D simulation. A simulation using

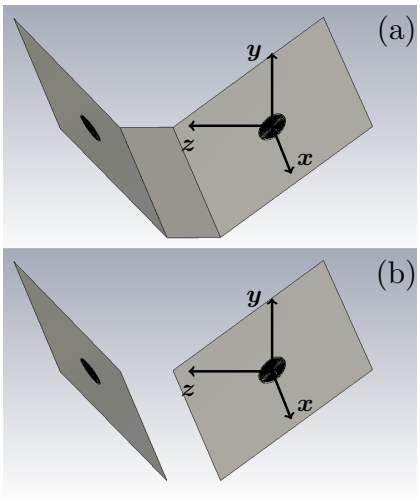

Figure 5.2: Spiral antennas on electrically large conducting planes which are (a) connected and (b) in free space. The opening angle between the antenna planes is $2\chi = 90°$.

the time-domain solver (FDTD) in CST verified that the difference in mutual coupling between the two cases (a) and (b) is small. The root mean square (RMS) error between the two curves is only 2 dB according to Fig. 5.3.

The antenna separation in this simulation is $d = 30$ cm (10λ for 10 GHz) and we choose a system of coordinates such that $R = 0$ according to Fig. 2.3. Since the conducting plane around each antenna is radiating, the effective size of each respective antenna is much larger than the antenna itself and it is not straightforward to define the radii ρ_{t} and ρ_{r} according to Fig. 2.3. Since these antennas are much larger than the previously considered ones, we can not expect to find a good agreement using Friis transmission equation at this considered distance. Indeed, the RMS error using Friis transmission equation is 24 dB according to Fig. 5.3.

There are several possible choices of far-fields when evaluating the NSCI (2.41). One choice to use the far-field found from the simulation of the original geometry (Fig. 5.2(a)). This far-field is referred to as the perturbed far-field. Another choice of far-field is the far-field of the spiral antenna with its adjacent conducting plane when the other is not present (i.e. one of the two disjunct structures in Fig. 5.2(b)). Perturbed far-fields typically vary more rapidly in the spherical angles than the unperturbed far-field. Hence, a smaller sample spacing is required in order to correctly sample this far-field according to the sampling theorem [31]. The mutual coupling was calculated for a total of 50 equidistantly spaced frequency samples and a piecewise cubic spline interpolation was used when presenting the results in Fig. 5.3. A reasonable agreement was found between the mutual coupling calculated with CST and calculated with the NSCI

(2.41) using both choices of far-fields. As can be seen in Fig. 5.3, using the perturbed far-field rather than the unperturbed far-field does not improve the estimation of the mutual coupling when sampling both far-fields with the same sample spacing. The RMS error is 6 dB when using the perturbed far-fields and 4 dB when using the unperturbed far-fields.

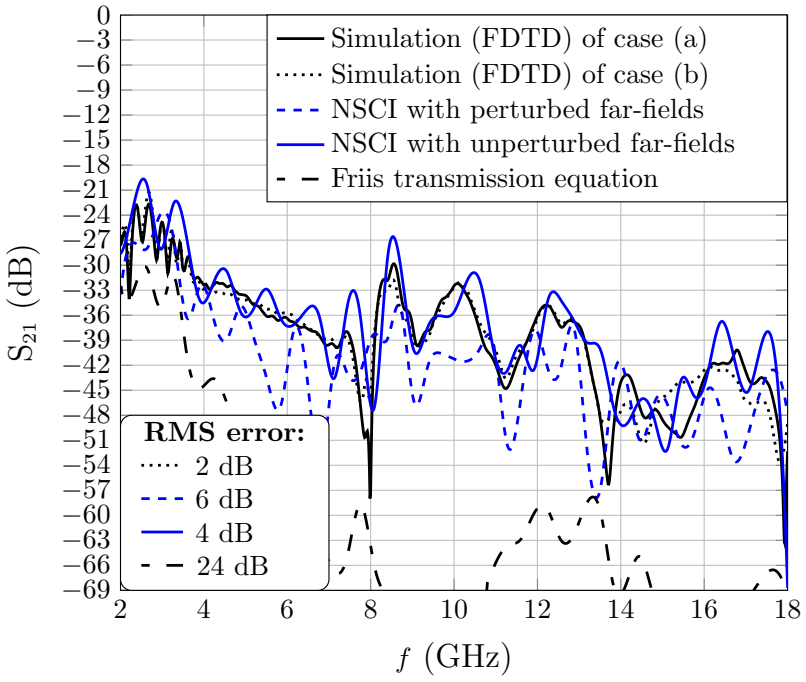

Figure 5.3: Mutual coupling between the antennas in Fig. 5.2 calculated using different methods.

Finally, we consider the geometry presented in Fig. 5.4 and calculate the mutual coupling as function of the opening angle 2χ between the antenna planes for the center frequency 10 GHz. When $2\chi > 180°$, the antennas no longer have visual contact. There are several such configurations on an aircraft. A similar problem for an aircraft could be to calculate the mutual coupling between antennas installed on on the respective wings of the aircraft such that the antennas do not have visual contact. The conducting planes in this simulation were chosen to be larger than in the preceding geometry presented in Fig. 5.2 where $d = 10\lambda$ for the center frequency 10 GHz. The antenna separation d varied from 10λ for $2\chi = 0°$ to 30λ for $2\chi = 180°$. The sample spacing 0.25° was chosen when sampling the far-field and the resulting dot product was interpolated before calculating the integral. The results from multi level fast multipole method (MLFMM) simulation using CST and numerical integration of the NSCI are presented in Fig. 5.5. The number of surface elements in this simulation was

roughly $80 \cdot 10^3$ and each simulation (i.e. each MLFMM data point in Fig. 5.5) takes roughly $24 - 50$ hours to calculate on a modern workstation. The results in Fig. 5.5 are therefore only presented for one single frequency. The numerical integration of the NSCI (2.41) on the other hand takes only a couple of minutes to calculate when the evaluation is parallelized and the same workstation is used.

A reasonable agreement was found between the simulation results and the NSCI in both the region with visual contact and the region without visual contact (Fig. 5.5). The RMS error using the NSCI is 9 dB whereas the RMS error using Friis transmission equation is 24 dB. The number of data points in Fig. 5.5 is very limited and only one frequency is considered. One should therefore be careful when drawing conclusions based on Fig. 5.5. These results will be discussed further in the following chapter.

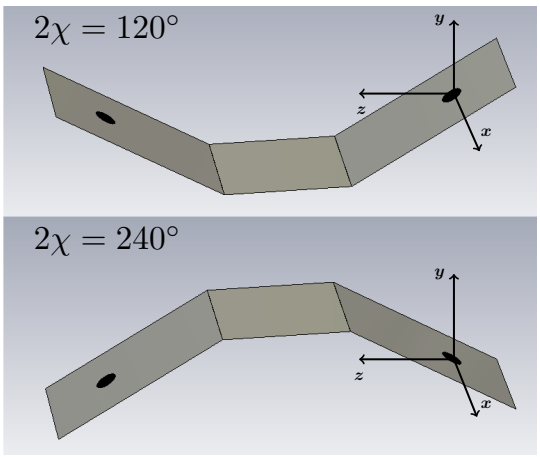

Figure 5.4: A vehicle similar to the one presented in Fig. 5.2 for some opening angles 2χ between the antenna planes.

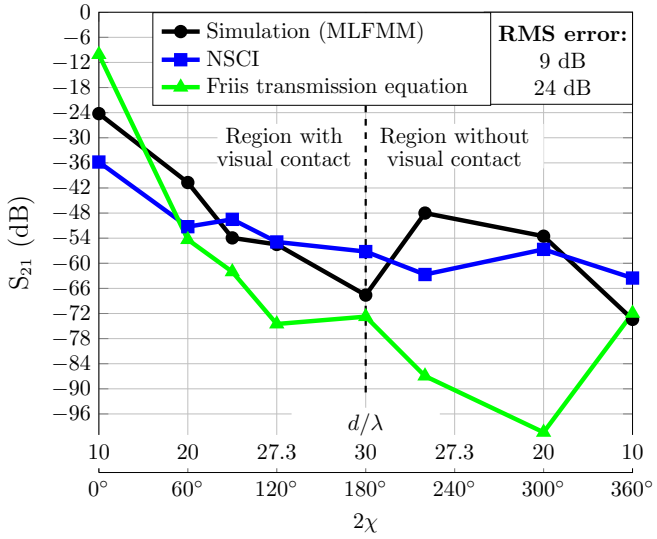

Figure 5.5: Mutual coupling between the antennas in Fig. 5.4 as function of the opening angle between antenna planes 2χ. The corresponding antenna separations d have been marked in the figure.

Chapter 6

Discussion and conclusion

The near-field generalization of Friis transmission equation (2.9) proposed by Yaghjian [7] has been investigated in this thesis by considering a large number of examples. A series expansion of this integral was derived for the time dependence $e^{j\omega t}$ following [7]. The most important result in this thesis is the change of variables which resulted in the non-singular coupling integral (2.41). Another important problem which was solved in this thesis was how to calculate the dot product $\boldsymbol{f}_{\mathrm{r}}(-\boldsymbol{k}) \cdot \boldsymbol{f}_{\mathrm{t}}(\boldsymbol{k})$ for sampled far-fields. It was shown in Section 4.4 that this dot product can be evaluated using $\boldsymbol{f}_{\mathrm{r}}(-\boldsymbol{k}) \cdot \boldsymbol{f}_{\mathrm{t}}(\boldsymbol{k}) = \boldsymbol{f}_{\mathrm{r}}(A\boldsymbol{k})^* \cdot \boldsymbol{f}_{\mathrm{t}}(\boldsymbol{k})$. Hence, the ratio of received to transmitted power between two antennas located in each others near-field can be calculated as the square magnitude of the non-singular coupling integral

$$\boxed{\left(\frac{b_{\mathrm{r}}}{a_{\mathrm{t}}}\right)_+ = \int_0^{\pi/2} d\theta \int_0^{2\pi} d\phi \; \boldsymbol{f}_{\mathrm{r}}(A\boldsymbol{k})^* \cdot \boldsymbol{f}_{\mathrm{t}}(\boldsymbol{k}) e^{-j\boldsymbol{K}\cdot\boldsymbol{R}} e^{-jkd\cos\theta} \sin\theta} \tag{6.1}$$

where $\boldsymbol{f}_{\mathrm{t}}$ and $\boldsymbol{f}_{\mathrm{r}}$ are the far-fields of the receiving and transmitting antennas respectively, $\boldsymbol{P} = \boldsymbol{R} + \hat{\boldsymbol{z}}d$ is the antenna separation and $\boldsymbol{K} \cdot \boldsymbol{R} = (kR_x \cos\phi + kR_y \sin\phi)\sin\theta$. This non-singular form of the coupling integral is, to the author's best knowledge, a novel contribution of this work to the current literature. The time dependence $e^{j\omega t}$ is assumed in (6.1). A normalization of the far-fields (2.16) was derived in order to take thermal and reflection losses into account in (6.1). There are two main advantages in using (6.1) rather than (2.38) from [7]. Firstly, this integral has greater numerical stability since it does not suffer from the singularity in $\gamma \equiv k_z = 0$. There is therefore no need to truncate the integration domain further than $K < k$, as done in [7]. Secondly, using $\boldsymbol{f}_{\mathrm{r}}(-\boldsymbol{k}) \cdot \boldsymbol{f}_{\mathrm{t}}(\boldsymbol{k}) = \boldsymbol{f}_{\mathrm{r}}(A\boldsymbol{k})^* \cdot \boldsymbol{f}_{\mathrm{t}}(\boldsymbol{k})$ it is possible to facilitate the evaluation of the dot product, as done in (6.1).

The non-singular coupling integral (6.1) has been demonstrated to agree well with simulation results for a large number of examples. In particular, a good

agreement has been found for circularly polarized antennas. This is a significant improvement compared to earlier computer programs which could only be used for linearly polarized and polarization-matched antennas [18].

It has been demonstrated through several examples in Chapter 3 and Chapter 4 that the non-singular coupling integral (6.1) is valid for smaller separation distances than the series expansion (2.39). This is due the fact that the convergence of the series expansion is limited by (2.35). It should however be noted that (6.1) is computationally heavy for extremely large separation distances and the series expansion (2.39) is advantageous in these cases. Furthermore, it was demonstrated in Chapter 5 that it is possible to calculate the mutual coupling as function of frequency using (6.1).

It has also been demonstrated that the non-singular coupling integral (6.1) can be used to find approximate values of the mutual coupling between antennas on vehicles. The approximation lies in the fact that the antennas are not truly in free space. If measured or calculated antenna far-fields are available with an appropriate sample spacing (*e.g.* $\leq 0.25^\circ$), then an estimation of the mutual coupling can be found using this method. It was demonstrated in the previous chapter that errors up to 9 dB can be expected using this method. The computational time required to calculate (6.1) in the last example in Chapter 5 was a few minutes on a modern workstation whereas the corresponding full three-dimensional simulation required $24 - 50$ hours per data point. This extreme difference in computational time is the main advantage in using this approximation.

The results in Fig. 5.5 indicate that a reasonable agreement is found also when the antennas do not have visual contact. The number of data points in Fig. 5.5 is however very limited and only one frequency is considered. Further work should therefore be aimed at investigating additional examples of aircraft-related problems to see if a good agreement is found for additional cases where the antennas do not have visual contact. Since it is expensive and time-consuming to measure or calculate antenna far-fields with a small sample spacing, it is also of interest to investigate methods to improve the integration performance for sparsely sampled far-fields. Furthermore, it could be interesting to investigate the effects of including evanescent modes in the integration domain. Finally, the results from this thesis will be submitted to a scientific journal.

Index

Bibliography

[1] J. D. Jackson, *Classical Electrodynamics*. 3rd edition, 1999, ch. 8-10.

[2] C. A. Balanis, *Antenna Theory, Analysis and Design*. 3rd edition, 2005, Wiley, ch. 2.17,3.8,4.1,4.6,8.6,10.3,12.9,AVIII.

[3] R. E. Collin, *Foundations for Microwave Engineering*. 2nd edition, 1992, McGraw-Hill, ch. 4.7.

[4] C. A. Balanis, *Modern Antenna Handbook*. 2008, Wiley, ch. 19.

[5] D. M. Kerns and E. S. Dayhoff, "Theory of diffraction in microwave interferometry," J. Res. Natl. Bur. Stand., Vol. 64B, pp. 1–13, January–March 1960.

[6] A. D. Yaghjian, "An overview of near-field antenna measurements," IEEE Transactions on Antennas and Propoagation, Vol. 34, No. 1, 1986.

[7] A. D. Yaghjian, "Efficient computation of antenna coupling and fields within the near-field region," *IEEE Transactions on Antennas and Propagation*, vol. AP-30, no. 1, 1982.

[8] D. M. Kerns, *Plane-Wave Scattering-Matrix Theory of Antennas and Antenna-Antenna Interactions*. Nat. Bur. Stand. Monograph 162, 1981.

[9] J. E. Hansen, *Spherical Near-Field Antenna Measurements*. IET Electromagnetic Waves Series 26, 1988.

[10] R. L. Lewis and A. C. Newell, "Efficient and accurate method for calculating and representing power density in the near zone of microwave antennas," IEEE Transactions on Antennas and Propoagation, Vol. 36, No. 6, 1988.

[11] K. Persson, M. Gustafsson, G. Kristensson, and B. Widenberg, "Radome diagnostics - source reconstruction of phase objects with an equivalent currents approach," IEEE Transactions on Antennas and Propagation, Vol. 62, No. 4, pp. 2041-2051, 2014.

[12] K. Persson, M. Gustafsson, and G. Kristensson, "Reconstruction and visualization of equivalent currents on a radome using an integral representation formulation," Progress in Electromagnetic Research B, Vol 20, pp.65-90, 2010.

[13] K. Persson, M. Gustafsson, G. Kristensson, and B. Widenberg, "Source reconstruction by far-field data for imaging of defects in frequency selective radomes," IEEE Transactions on Antennas and Propagation, Vol. 62, No. 4, pp. 2041-2051, 2014.

[14] Q. Haichao, Q. Haichao, S. Donglin, S. Donglin, L. Ying, and L. Ying, "Research of the testing method of radiation pattern for on-board installed antennas," 2008 8th International Symposium on Antennas, Propagation and EM Theory, Nov. 2008, pp.1139-1141.

[15] H. T. Friis, "A note on a simple transmission formula," Proc. IRE, vol. 34, no. 5, pp. 254–256, 1946.

[16] I. Kim, S. Xu, Y. Rahmat-Samii, and H. Eyyuboglu, "Generalised correction to the friis formula: quick determination of the coupling in the fresnel region," IET Microwaves, Antennas and Propagation, 2013.

[17] Y.-S. Cheng, S.-Y. Chen, and H.-J. Li, "Analysis of antenna coupling in near-field communication systems," IEEE Transactions on Antennas and Propagation, Vol. 58, No. 10, 2010, pp. 3327-3335.

[18] C. F. Stubenrauch and M. H. Francis, "Comparison of measured and calculated mutual coupling in the near field between microwave antennas," IEEE Transactions on Antennas and Propagation, Vol AP-34, No. 7, 1986, pp.952-955.

[19] M. H. Francis and C. F. Stubenrauch, "Comparison of measured and calculated antenna sidelobe coupling loss in the near field using approximate far-field data," IEEE Transactions on Antennas and Propoagation, Vol. 36, No. 3, 1988.

[20] A. H. Akgiray and Y. Rahmat-Samii, "Mutual coupling between two arbitrarily oriented and positioned antennas in near- and far-field regions," 2010 URSI International Symposiom on Electromagnetic Theory, pp. 780-783.

[21] *CST Microwave Studio documentation.* 2014, `www.cst.com`.

[22] E. M. Stein and R. Shakarchi, *Fourier Analysis, An Introduction.* Princeton University Press, 2003, pp. 129,176.

[23] A. Vretblad, *Fourier Analysis and Its Applications.* Springer, 2000, pp. 165.

[24] D. H. Bailey and P. N. Swarztrauber, "A fast method for the numerical evaluation of continuous fourier and laplace transforms," J. on Scientific Computing, vol. 15, no. 5 (Sept. 1994), pp.1105-1110.

[25] E. O. Brigham, *The Fast Fourier Transform and its Applications*. Prentice-Hall, 1988.

[26] P. C. Matthews, *Vector Calculus*. Springer, 7th printing 2005, pp. 72.

[27] B. L. G. Jonsson and S. Ström, *Electromagnetic wave propagation and scattering*. Kungliga Tekniska Högskolan 2013.

[28] J. A. Stratton, *Electromagnetic Theory*. New York: MCGraw-Hill, 1941, ch. 7.

[29] L. Råde and B. Westergren, *Mathematics Handbook for Science and Engineering*. 5th edition, pp.248,315.

[30] M. Norgren, *EI1240 TET F - grundläggande om antenner*. Electronic lecture notes in the course EI1240 at Kungliga Tekniska Högskolan, 2012.

[31] P. Händel, R. Ottosson, and H. Hjalmarsson, *Signalteori*. 3rd edition, 2002, ISBN 91-974087-2-7 (available in English).

[32] E. Sermutlu and H. Eyyuboglu, "A new quadrature routine for improper and oscillatory integrals," Applied Mathematics and Computation 189 (2007) 452–461, pp. 1092-1101.

[33] *MATLAB documentation*. 2014, `www.mathworks.se`.

[34] B. N. Miller and D. L. Ranum, *Problem Solving with Algorithms and Data Structures using Python*. 2006, Franklin, Beedle and Associates Incorporated.

[35] *Wolfram Mathematica*. 2014, `www.wolfram.com`.

Appendix A

List of source code

The source code developed as part of this thesis has been organized using general principles in computer science found in a large number of textbooks, e.g. [34]. All important routines have been implemented as separate functions, thus creating an interface between the user and each routine. Furthermore, the consistent use of functions results in a clean source code where the same code is not repeated unnecessarily. The source code developed as part of this thesis is organized in a number of folders:

- LIBRARY - This folder contains all functions that are commonly used in this thesis.
- DIPOLES - This folder contains the source code used in Section 3.1.
- APERTURES - This folder contains the source code used in Sections 3.2 and 4.3.
- HORNS - This folder contains the source code and data sets used in Section 4.5.
- SPIRALSPIRAL - This folder contains the source code and data sets used in Section 4.4.
- SPIRALHELIX - This folder contains the source code and data sets used in Section 4.6.
- SPIRALDIPOLE - This folder contains the source code and data sets used in Section 5.1.

Each folder contains a `README`-file which is intended to give an overview of the contents of each folder. The folder LIBRARY contains the following functions and programs:

Far-field data:

- `exportFF1.mcr` - This CST Macro is used to export the electric far-field to an ASCII file for an arbitrarily small sample spacing. The magnitude (dB) and phase (deg) are exported separately for the θ and ϕ polarizations.
- `exportFF2.mcr` - This CST Macro is used to export the electric far-field to an ASCII file for an arbitrarily small sample spacing. The real and imaginary parts are exported separately for the θ and ϕ polarizations.
- `createFFminitors.mcr` - This CST Macro is used to quickly create an arbitrarly large number of far-field monitors.
- `loadFarField.m` - This Matlab function is used to import far-fields which are exported using `exportFF2.mcr`. This file also imports the frequency from the ASCII file.
- `readline.m` - This Matlab function reads one line from an ASCII file. Hence, information can be quickly be extracted from large ASCII files without loading the entire file.
- `removeheader.m` - This Matlab function removes the header from a large text file such that it can be loaded by the Matlab function `load`.
- `getData.m` - This Matlab function is used to search ASCII files for relevant data, which is useful when analyzing the result from a parametric sweep.

Special functions:

- `legendrePol.m` - Legendre polynomials.
- `hankel1.m` - Spherical Hankel functions of the first kind.
- `hankel2.m` - Spherical Hankel functions of the second kind.
- `sphericalbesselj.m` - Spherical Bessel functions.
- `sphericalbessely.m` - Spherical Neumann functions.
- `spharm.m` - Spherical harmonic functions.

Visualization:

- `plotDirectivity3D.m` - 3D directivity (or gain) plot in Matlab.
- `tikzdata.m` - This function exports two vectors to an ASCII file in a format which can be used by Tikz for Latex.

Coupling program:

- `CouplingProgramDirect.m` - This program calculates the mutual coupling between two antennas using the non-singular coupling integral (2.41).

- `CouplingProgramSeries.m` - This program calculates the mutual coupling between two arbitrary antennas using the series expansion (2.39).
- `CouplingProgramSeriesFast.m` - This program calculates the mutual coupling between two arbitrary antennas using the series expansion (2.39) and the fast method of integration from Section 4.1.
- `CouplingProgramFrequency.m` - This program calculates the mutual coupling between two arbitrary antennas as function of frequency using the non-singular coupling integral (2.41).
- `postprocess.m` - This script plots the results from the coupling program together with the results from Friis transmission equation. The script can also plot simulation results from CST in the same figures.

Appendix B

On the normalized vector far-field function f

The antenna far-fields can be represented by the normalized vector far-field function $\boldsymbol{f}(\hat{\boldsymbol{r}})$ according to (2.2). This normalization is motivated by the relation

$$\lim_{r\to\infty} \boldsymbol{E}(\boldsymbol{r}) = \frac{e^{-jkr}}{r} V_0 \boldsymbol{f}(\hat{\boldsymbol{r}})$$

which holds for any electric field $\boldsymbol{E}(\boldsymbol{r})$ which is generated by a source bounded by a sphere of radius R. This relation will now be proven. The time convention $e^{j\omega t}$ is assumed in this appendix. $\boldsymbol{E}(\boldsymbol{r})$ can be expressed as a multipole expansion in the exterior region $r > R$ [1, 27]:

$$\begin{aligned}\boldsymbol{E}(\boldsymbol{r}) = \sum_{l=1}^{\infty}\sum_{m=-l}^{l}\Bigg[& a_{lm}^{(M)}\sqrt{l(l+1)}\mathrm{h}_l^{(2)}(kr)\boldsymbol{X}_{lm}^1(\theta,\phi) \\ & + Z_0 a_{lm}^{(E)}\left(-j\frac{\sqrt{l(l+1)}}{kr}\left(1+r\frac{\partial}{\partial r}\right)\mathrm{h}_l^{(2)}(kr)\boldsymbol{X}_{lm}^2(\theta,\phi)\right. \\ & \left.\left. + \frac{l(l+1)}{kr}\mathrm{h}_l^{(2)}(kr)\boldsymbol{X}_{lm}^3(\theta,\phi)\right)\right]\end{aligned} \tag{B.1}$$

where $a_{lm}^{(M)}$ and $a_{lm}^{(E)}$ are some coefficients and the vector spherical harmonic functions are given by:

$$\boldsymbol{X}_{lm}^1(\theta,\varphi) = \boldsymbol{L}\frac{1}{\sqrt{l(l+1)}}\mathrm{Y}_{lm}(\theta,\varphi) \tag{B.2}$$

$$\boldsymbol{X}_{lm}^2(\theta,\varphi) = \hat{\boldsymbol{r}}\times\boldsymbol{X}_{lm}^1(\theta,\varphi) = \hat{\boldsymbol{r}}\times\boldsymbol{L}\frac{1}{\sqrt{l(l+1)}}\mathrm{Y}_{lm}(\theta,\varphi) \tag{B.3}$$

$$\boldsymbol{X}_{lm}^3(\theta,\varphi) = \hat{\boldsymbol{r}}\mathrm{Y}_{lm}(\theta,\varphi) \tag{B.4}$$

where $\boldsymbol{L} \equiv -j(\boldsymbol{r} \times \nabla)$ is $\hbar^{-1}$ times the orbital angular momentum operator. It is well-known that the electric far-field does not have an $\hat{\boldsymbol{r}}$-component [1,2] and the terms including $\boldsymbol{X}^3_{lm}$ in (B.1) will therefore not contribute to the far-field. In the antenna far-field region we thus have

$$\begin{aligned}\boldsymbol{E}(\boldsymbol{r}) = \sum_{l=1}^{\infty}\sum_{m=-l}^{l}\Bigg[& a^{(M)}_{lm}\sqrt{l(l+1)}\mathrm{h}^{(2)}_l(kr)\boldsymbol{X}^1_{lm}(\theta,\phi) \\ & - jZ_0 a^{(E)}_{lm}\frac{\sqrt{l(l+1)}}{kr}\left(1 + r\frac{\partial}{\partial r}\right)\mathrm{h}^{(2)}_l(kr)\boldsymbol{X}^2_{lm}(\theta,\phi)\Bigg]\end{aligned} \tag{B.5}$$

Furthermore, the derivative of the spherical Hankel function in (B.1) may be expanded (see e.g. [35]):

$$\frac{\partial}{\partial kr}\mathrm{h}^{(2)}_l(kr) = e^{-jkr}\left(\frac{e^{jl\pi/2}}{kr} + O((kr)^{-2})\right) \tag{B.6}$$

where Ordo is denoted by O. Substituting (B.6) and (2.25) into (B.5) yields:

$$\begin{aligned}\lim_{r\to\infty}\boldsymbol{E}(\boldsymbol{r}) &= \sum_{l=1}^{\infty}\sum_{m=-l}^{l}\Bigg[a^{(M)}_{lm}\sqrt{l(l+1)}j^{l+1}\frac{e^{-jkr}}{kr}\boldsymbol{X}^1_{lm}(\theta,\phi) \\ &\qquad - jZ_0 a^{(E)}_{lm}\sqrt{l(l+1)}e^{-jkr}\frac{j^l}{kr}\boldsymbol{X}^2_{lm}(\theta,\phi)\Bigg] \\ &= \frac{e^{-jkr}}{r}V_0\boldsymbol{f}(\hat{\boldsymbol{r}})\end{aligned} \tag{B.7}$$

and the proof is thus complete. Finally, the normalized vector far-field function can be identified:

$$V_0\boldsymbol{f}(\hat{\boldsymbol{r}}) = \sum_{l=1}^{\infty}\sum_{m=-l}^{l}\sqrt{l(l+1)}j^{l+1}k^{-1}\left[a^{(M)}_{lm}\boldsymbol{X}^1_{lm}(\hat{\boldsymbol{r}}) - Z_0 a^{(E)}_{lm}\boldsymbol{X}^2_{lm}(\hat{\boldsymbol{r}})\right]. \tag{B.8}$$